1

Spaser, Plasmonic Amplification, and Loss Compensation

MARK I. STOCKMAN
Department of Physics and Astronomy, Georgia State University, Atlanta, Georgia, USA

1.1 INTRODUCTION TO SPASERS AND SPASING

Not just a promise anymore [1], nanoplasmonics has delivered a number of important applications: ultrasensing [2], scanning near-field optical microscopy [3, 4], surface plasmon (SP)-enhanced photodetectors [5], thermally assisted magnetic recording [6], generation of extreme UV (EUV) [7], biomedical tests [2, 8], SP-assisted thermal cancer treatment [9], plasmonic-enhanced generation of EUV pulses [7] and extreme ultraviolet to soft x-ray (XUV) pulses [10], and many others—see also Reference 11 and 12.

To continue its vigorous development, nanoplasmonics needs an active device—near-field generator and amplifier of nanolocalized optical fields, which has until recently been absent. A nanoscale amplifier in microelectronics is the metal-oxide-semiconductor field effect transistor (MOSFET) [13, 14], which has enabled all contemporary digital electronics, including computers and communications, and the present-day technology as we know it. However, the MOSFET is limited by frequency and bandwidth to $\lesssim 100$ GHz, which is already a limiting factor in further technological development. Another limitation of the MOSFET is its high sensitivity to temperature, electric fields, and ionizing radiation, which limits its use in extreme environmental conditions and nuclear technology and warfare.

An active element of nanoplasmonics is the spaser (Surface Plasmon Amplification by Stimulated Emission of Radiation), which was proposed [15, 16] as a nanoscale quantum generator of nanolocalized coherent and intense optical fields. The idea of spaser has been further developed theoretically [17–26]. Spaser effect has recently

Active Plasmonics and Tuneable Plasmonic Metamaterials, First Edition. Edited by Anatoly V. Zayats and Stefan A. Maier.
 Published 2013 by John Wiley & Sons, Inc.

been observed experimentally [27]. Also a number of surface plasmon polariton (SPP) spasers (also called nanolasers) have been experimentally observed [28–33], see also References 34–37. Closely related to the spaser are nanolasers built on deep subwavelength metal nanocavities [38, 39].

1.2 SPASER FUNDAMENTALS

Spaser is a nanoplasmonic counterpart of laser [15, 17]: It is a quantum generator and nanoamplifier where photons as the participating quanta are replaced by SPs. Spaser consists of a metal nanoparticle, which plays the role of a laser cavity (resonator), and the gain medium. Figure 1.1 schematically illustrates the geometry of a spaser as introduced in the original article [15], which contains a V-shaped metal nanoparticle surrounded by a layer of semiconductor nanocrystal quantum dots (QDs).

The laser has two principal elements: resonator (or cavity) that supports photonic mode(s) and the gain (or active) medium that is population-inverted and supplies energy to the lasing mode(s). An inherent limitation of the laser is that the size of the laser cavity in the propagation direction is at least half the wavelength and practically more than that even for the smallest lasers developed [28, 29, 40].

In a true spaser [15, 18], this limitation is overcome. The spasing modes are SPs whose localization length is on the nanoscale [41] and is only limited by the minimum inhomogeneity scale of the plasmonic metal and the nonlocality radius [42] $l_{nl} \sim 1$ nm. This nonlocality length is the distance that an electron with the Fermi velocity v_F moves in space during a characteristic period of the optical field:

$$l_{nl} \sim v_F/\omega \sim 1 \text{ nm}, \tag{1.1}$$

where ω is the optical frequency, and the estimate is shown for the optical spectral region. So, the spaser is truly nanoscopic—its minimum total size can be just a few nanometers.

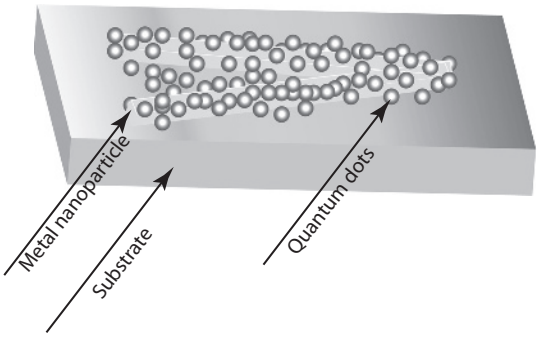

FIGURE 1.1 Schematic of the spaser as originally proposed in Reference 15. The resonator of the spaser is a metal nanoparticle shown as a gold V-shape. It is covered by the gain medium depicted as nanocrystal quantum dots. This active medium is supported by a neutral substrate.

The resonator of a spaser can be any plasmonic metal nanoparticle whose total size R is much less than the wavelength λ and whose metal thickness is between l_{nl} and l_s, which supports an SP mode with required frequency ω_n. Here l_s is the skin depth:

$$l_s = \bar{\lambda}\left[\mathrm{Re}\left(\frac{-\varepsilon_m^2}{\varepsilon_m+\varepsilon_d}\right)^{1/2}\right]^{-1}, \tag{1.2}$$

where $\bar{\lambda} = \lambda/(2\pi) = \omega/c$ is the reduced vacuum wavelength, ε_m is the dielectric function (or, permittivity) of the metal, and ε_d is that of the embedding dielectric. For single-valence plasmonic metals (silver, gold, copper, alkaline metals) $l_s \approx 25$ nm in the entire optical region.

This metal nanoparticle should be surrounded by the gain medium that overlaps with the spasing SP eigenmode spatially and whose emission line overlaps with this eigenmode spectrally [15]. As an example, we consider in more detail a model of a nanoshell spaser [17, 18, 43], which is illustrated in Figure 1.2. Panel (a) shows a silver nanoshell carrying a single SP (plasmon population number $N_n = 1$) in the dipole eigenmode. It is characterized by a uniform field inside the core and hot spots at the poles outside the shell with the maximum field reaching $\sim 10^6$ V/cm. Similarly, Figure 1.2b shows the quadrupole mode in the same nanoshell. In this case, the mode electric field is nonuniform, exhibiting hot spots of $\sim 1.5 \times 10^6$ V/cm of the modal electric field at the poles. These high values of the modal fields, which are related to the small modal volume, are the underlying physical reason for a very strong feedback in the spaser. Under our conditions, the electromagnetic retardation within the spaser volume can be safely neglected. Also, the radiation of such a spaser is a weak effect: The decay rate of plasmonic eigenmodes is dominated by the internal loss in the metal. Therefore, it is sufficient to consider only quasistatic eigenmodes [41, 44] and not their full electrodynamic counterparts [45].

For the sake of numerical illustrations of our theory, we will use the dipole eigenmode (Fig. 1.2a). There are two basic ways to place the gain medium: (i) outside the nanoshell, as shown in panel (c), and (ii) in the core, as in panel (d), which was originally proposed in Reference 43. As we have verified, these two designs lead to comparable characteristics of the spaser. However, the placement of the gain medium inside the core illustrated in Figure 1.2d has a significant advantage because the hot spots of the local field are not covered by the gain medium and are sterically available for applications.

Note that any l-multipole mode of a spherical particle is, indeed, $2l + 1$-times degenerate. This may make the spasing mode to be polarization unstable, like in lasers without polarizing elements. In reality, the polarization may be clamped and become stable due to deviations from the perfect spherical symmetry, which exist naturally or can be introduced deliberately. More practical shape for a spaser may be a nanorod [24], which has a mode with the stable polarization along the major axis. However, a nanorod is a more complicated geometry for theoretical treatment.

The level diagram of the spaser gain medium and the plasmonic metal nanoparticle is displayed in Figure 1.2e along with a schematic of the relevant energy transitions in

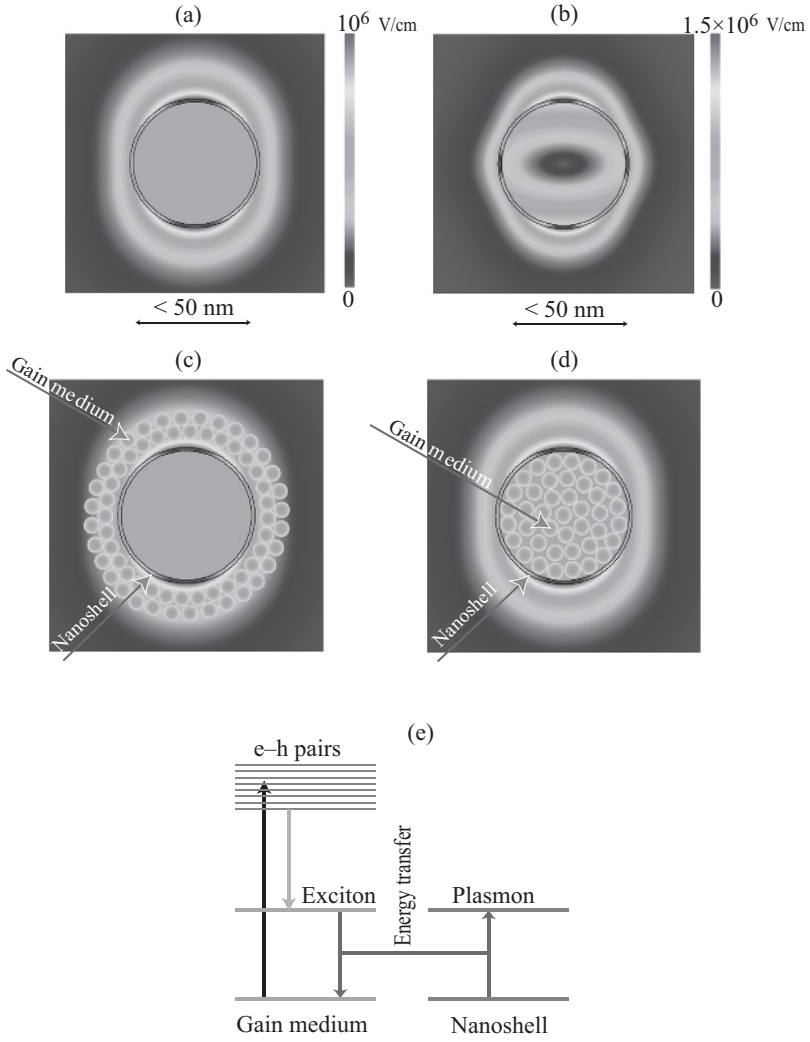

FIGURE 1.2 Schematic of spaser geometry, local fields, and fundamental processes leading to spasing. (a) Nanoshell geometry and the local optical field distribution for one SP in an axially symmetric dipole mode. The nanoshell has aspect ratio $\eta = 0.95$. The local-field magnitude is color-coded by the scale bar in the right-hand side of the panel. (b) The same as (a) but for a quadrupole mode. (c) Schematic of a nanoshell spaser where the gain medium is outside of the shell, on the background of the dipole-mode field. (d) The same as (c) but for the gain medium inside the shell. (e) Schematic of the spasing process. The gain medium is excited and population-inverted by an external source, as depicted by the black arrow, which produces electron–hole pairs in it. These pairs relax, as shown by the green arrow, to form the excitons. The excitons undergo decay to the ground state emitting SPs into the nanoshell. The plasmonic oscillations of the nanoshell stimulate this emission, supplying the feedback for the spaser action. Adapted from Reference 18.

the system. The gain medium chromophores may be semiconductor nanocrystal QDs [15, 46], dye molecules [47, 48], rare-earth ions [43], or electron–hole excitations of an unstructured semiconductor [28, 40]. For certainty, we will use a semiconductor-science language of electrons and holes in QDs.

The pump excites electron–hole pairs in the chromophores (Fig. 1.2e), as indicated by the vertical black arrow, which relax to form excitons. The excitons constitute the two-level systems that are the donors of energy for the SP emission into the spasing mode. In vacuum, the excitons would recombine emitting photons. However, in the spaser geometry, the photoemission is strongly quenched due to the resonance energy transfer to the SP modes, as indicated by the red arrows in the panel. The probability of the radiativeless energy transfer to the SPs relative to that of the radiative decay (photon emission) is given by the so-called Purcell factor

$$\sim \frac{\bar{\lambda}^3 Q}{R^3} \gg 1, \tag{1.3}$$

where R is a characteristic size of the spaser metal core and Q is the plasmonic quality factor [12], and $Q \sim 100$ for a good plasmonic metal such as silver. Thus, this radiativeless energy transfer to the spaser mode is the dominant process whose probability is by orders of magnitude greater than that of the free-space (far-field) emission.

The plasmons already in the spaser mode create the high local fields that excite the gain medium and stimulate more emission to this mode, which is the feedback mechanism. If this feedback is strong enough, and the lifetime of the spaser SP mode is long enough, then an instability develops leading to the avalanche of the SP emission in the spasing mode and spontaneous symmetry breaking, establishing the phase coherence of the spasing state. Thus the establishment of spasing is a nonequilibrium phase transition, as in the physics of lasers.

1.2.1 Brief Overview of the Latest Progress in Spasers

After the original theoretical proposal and prediction of the spaser [15], there has been an active development in this field, both theoretical [17–26] and experimental [27–33]; see also [11, 12]. There has also been a US patent issued on spaser [16].

Among theoretical developments, a nanolens spaser has been proposed [49], which possesses a nanofocus (“the hottest spot”) of the local fields. In References 15 and 49, the necessary condition of spasing has been established on the basis of the perturbation theory.

There have been theories published describing the SPP spasers (or “nanolasers” as sometimes they are called) phenomenologically, on the basis of classic linear electrodynamics by considering the gain medium as a dielectric with a negative imaginary part of the permittivity (e.g., [43]). Very close fundamentally and technically are works on the loss compensation in metamaterials [50–53]. Such linear-response approaches do not take into account the nature of the spasing as a nonequilibrium phase transition, at the foundation of which is spontaneous symmetry breaking: establishing coherence

with an arbitrary but sustained phase of the SP quanta in the system [18]. Spaser is necessarily a deeply nonlinear (nonperturbative) phenomenon where the coherent SP field always saturates the gain medium, which eventually brings about establishment of the stationary [or continuous wave (CW)] regime of the spasing [18]. This leads to principal differences of the linear-response results from the microscopic quantum-mechanical theory in the region of spasing, as we discuss below in conjunction with Figure 1.4.

There has also been a theoretical publication on a bow tie spaser (nanolaser) with electrical pumping [54]. It is based on balance equations and only the CW spasing generation intensity is described. Yet another theoretical development has been a proposal of the lasing spaser [55], which is made of a plane array of spasers.

There has also been a theoretical proposal of a spaser ("nanolaser") consisting of a metal nanoparticle coupled to a single chromophore [56]. In this paper, a dipole–dipole interaction is illegitimately used at very small distances r where it has a singularity (diverging for $r \to 0$), leading to a dramatically overestimated coupling with the SP mode. As a result, a completely unphysical prediction of CW spasing due to single chromophore has been obtained [56]. In contrast, our theory [18] is based on the full (exact) field of the spasing SP mode without the dipole (or any multipole) approximation. As our results of Section 1.3.4 below show, hundreds of chromophores per metal nanoparticle are realistically required for the spasing even under the most favorable conditions.

There has been a vigorous experimental investigation of the spaser and the concepts of spaser. Stimulated emission of SPPs has been observed in a proof-of-principle experiment using pumped dye molecules as an active (gain) medium [47]. There have also been later experiments that demonstrated strong stimulated emission compensating a significant part of the SPP loss [48, 57–61]. As a step toward the lasing spaser, the first experimental demonstration has been reported of a partial compensation of the Joule losses in a metallic photonic metamaterial using optically pumped PbS semiconductor QDs [46]. There have also been experimental investigations reporting the stimulated emission effects of SPs in plasmonic metal nanoparticles surrounded by gain media with dye molecules [62, 63]. The full loss compensation and amplification of the long-range SPPs at $\lambda = 882$ nm in a gold nanostrip waveguide with a dye solution as a gain medium has been observed [64].

At the present time, there have been a considerable number of successful experimental observations of spasers and SPP spasers (also called nanolasers). An electrically pumped nanolaser with semiconductor gain medium has been demonstrated [28] where the lasing modes are SPPs with a one-dimensional (1d) confinement to a ~ 50 nm size. A nanolaser with an optically pumped semiconductor gain medium and a hybrid semiconductor/metal (CdS/Ag) SPP waveguide has been demonstrated with an extremely tight transverse (2d) mode confinement to ~ 10 nm size [29]. This has been followed by the development of a CdS/Ag nanolaser generating a visible single mode at room temperature with a tight 1d confinement (~ 20 nm) and a 2d confinement in the plane of the structure to an area $\sim 1\ \mu m^2$ [30]. A highly efficient SPP spaser in the communication range ($\lambda = 1.46\,\mu m$) with an optical pumping based on a gold film and an InGaAs semiconductor quantum-well gain medium has recently been reported [31]. Another nanolaser (spaser) has been reported based on

gold as a plasmonic metal and InGaN/GaN nanorods as gain medium [32]. This spaser generates in the green optical range. Also a promising type of spasers has been introduced [33] based on distributed feedback (DFB). The nanolaser demonstrated in Reference 33 generates at room temperature and has lower threshold than other spasers—see also the corresponding discussion in Section 1.4.6.

There has been an observation published of a nanoparticle spaser [27]. This spaser is a chemically synthesized gold nanosphere of radius 7 nm surrounded by a dielectric shell of 21 nm outer radius containing immobilized dye molecules. Under nanosecond optical pumping in the absorption band of the dye, this spaser develops a relatively narrow-spectrum and intense visible emission that exhibits a pronounced threshold in pumping intensity. The observed characteristics of this spaser are in an excellent qualitative agreement and can be fully understood on the basis of the corresponding theoretical results described in Section 1.3.4.

1.3 QUANTUM THEORY OF SPASER

1.3.1 Surface Plasmon Eigenmodes and Their Quantization

Here we will follow References 41, 65, and 66 to introduce SPs as eigenmodes and Reference 15 to quantize them. Assuming that a nanoplasmonic system is small enough, $R \ll \bar{\lambda}$, $R \lesssim l_s$, we employ the so-called quasistatic approximation where the Maxwell equations reduce to the continuity equation for the electrostatic potential $\varphi(\mathbf{r})$:

$$\frac{\partial}{\partial \mathbf{r}} \varepsilon(\mathbf{r}) \frac{\partial}{\partial \mathbf{r}} \varphi(\mathbf{r}) = 0. \tag{1.4}$$

The systems permittivity (dielectric function) varying in space and frequency-dependent is expressed as

$$\varepsilon(\mathbf{r}, \omega) = \varepsilon_m(\omega)\Theta(\mathbf{r}) + \varepsilon_d[1 - \Theta(\mathbf{r})] = \varepsilon_d \left[1 - \frac{\Theta(\mathbf{r})}{s(\omega)}\right]. \tag{1.5}$$

Here $\Theta(\mathbf{r})$ is the so-called characteristic function of the nanosystem, which is equal to 1 when $\mathbf{r}$ belongs to the metal and 0 otherwise. We have also introduced Bergman's spectral parameter [44]:

$$s(\omega) = \frac{\varepsilon_d}{\varepsilon_d - \varepsilon_m(\omega)}. \tag{1.6}$$

A classical-field SP eigenmode $\varphi_n(\mathbf{r})$ is defined by the following generalized eigenproblem, which is obtained from Equation (1.4) by substituting Equations (1.5) and (1.6):

$$\frac{\partial}{\partial \mathbf{r}} \Theta(\mathbf{r}) \frac{\partial}{\partial \mathbf{r}} \varphi_n(\mathbf{r}) - s_n \frac{\partial^2}{\partial \mathbf{r}^2} \varphi_n(\mathbf{r}) = 0, \tag{1.7}$$

where ω_n is the corresponding eigenfrequency and $s_n = s(\omega_n)$ is the corresponding eigenvalue.

To be able to carry out the quantization procedure, we must neglect losses, that is, consider a purely Hamiltonian system. This requires that we neglect $\operatorname{Im}\varepsilon_m$, which we do only in this subsection. Then the eigenvalues s_n and the corresponding SP wave functions φ_n, as defined by Equation (1.7), are all real. Note that for good metals in the plasmonic region, $\operatorname{Im}\varepsilon_m \ll |\operatorname{Re}\varepsilon_m|$, cf. Reference 12, so this procedure is meaningful.

The eigenfunctions $\varphi_n(\mathbf{r})$ satisfy the homogeneous Dirichlet–Neumann boundary conditions on a surface S surrounding the system. These we set as

$$\varphi_1(\mathbf{r})|_{\mathbf{r}\in S} = 0, \text{ or } \mathbf{n}(\mathbf{r})\frac{\partial}{\partial \mathbf{r}}\varphi_1(\mathbf{r})\bigg|_{\mathbf{r}\in S} = 0, \tag{1.8}$$

with $\mathbf{n}(\mathbf{r})$ denoting a normal to the surface S at a point of $\mathbf{r}$.

From Equations (1.4), (1.5), (1.6), (1.7), and (1.8) it is straightforward to obtain that

$$\int_V \varepsilon(\mathbf{r},\omega)\,|\nabla\varphi_n(\mathbf{r})|^2\,dV = \varepsilon_d\left[1 - \frac{s_n}{s(\omega)}\right], \tag{1.9}$$

where V is the volume of the system.

To quantize the SPs, we write the operator of the electric field of an SP eigenmode as a sum over the eigenmodes:

$$\hat{\mathbf{E}}(\mathbf{r}) = -\sum_n A_n \nabla\varphi_n(\mathbf{r})(\hat{a}_n + \hat{a}_n^\dagger), \tag{1.10}$$

where $\hat{a}_n^\dagger$ and $\hat{a}_n$ are the SP creation and annihilation operators, $-\nabla\varphi_n(\mathbf{r}) = \mathbf{E}_n(\mathbf{r})$ is the modal field of an nth mode, and A_n is an unknown normalization constant. Note that $\hat{a}_n^\dagger$ and $\hat{a}_n$ satisfy the Bose–Einstein canonical commutation relations,

$$\left[\hat{a}_n, \hat{a}_m^\dagger\right] = \delta_{mn}, \tag{1.11}$$

where δ_{mn} is the Kronecker symbol.

To find normalization constant A_n, we invoke Brillouin's expression [67] for the average energy $\langle\hat{H}_{SP}\rangle$ of SPs as a frequency-dispersive system:

$$\left\langle\hat{H}_{SP}\right\rangle = \frac{1}{8\pi}\int_V \frac{\partial}{\partial\omega}\left[\omega\varepsilon(\mathbf{r},\omega)\right]\sum_n \left\langle\hat{\mathbf{E}}_n^\dagger(\mathbf{r})\hat{\mathbf{E}}_n(\mathbf{r})\right\rangle dV, \tag{1.12}$$

where

$$\hat{H}_{SP} = \sum_n \hbar\omega_n\left(\hat{a}_n^\dagger\hat{a}_n + \frac{1}{2}\right) \tag{1.13}$$

is the SP Hamiltonian in the second quantization.

Finally, we substitute the field expansion (1.10) into Equation (1.12) and take into account Equation (1.9) to carry out the integration. Comparing the result with Equation (1.13), we immediately obtain an expression for the quantization constant:

$$A_n = \left(\frac{4\pi\hbar s_n}{\varepsilon_d s_n'}\right)^{1/2}, \; s_n' \equiv \mathrm{Re}\frac{ds(\omega)}{d\omega}\bigg|_{\omega=\omega_n} \tag{1.14}$$

Note that we have corrected a misprint in Reference 15 by replacing the coefficient 2π by 4π.

1.3.2 Quantum Density Matrix Equations (Optical Bloch Equations) for Spaser

Here we follow Reference 18. The spaser Hamiltonian has the form

$$\hat{H} = \hat{H}_g + \hat{H}_{SP} - \sum_p \hat{\mathbf{E}}(\mathbf{r}_p)\hat{\mathbf{d}}^{(p)}, \tag{1.15}$$

where $\hat{H}_g$ is the Hamiltonian of the gain medium, p is a number (label) of a gain medium chromophore, $\mathbf{r}_p$ is its coordinate vector, and $\hat{\mathbf{d}}^{(p)}$ is its dipole-moment operator. In this theory, we treat the gain medium quantum mechanically but the SPs quasi-classically, considering $\hat{a}_n$ as a classical quantity (c-number) a_n with time dependence as $a_n = a_{0n}\exp(-i\omega t)$, where a_{0n} is a slowly varying amplitude. The number of coherent SPs per spasing mode is then given by $N_p = |a_{0n}|^2$. This approximation neglects quantum fluctuations of the SP amplitudes. However, when necessary, we will take into account these quantum fluctuations, in particular, to describe the spectrum of the spaser.

Introducing $\rho^{(p)}$ as the density matrix of a pth chromophore, we can find its equation of motion in a conventional way by commutating it with the Hamiltonian (1.15) as

$$i\hbar\dot{\rho}^{(p)} = [\rho^{(p)}, \hat{H}], \tag{1.16}$$

where the dot denotes temporal derivative. We use the standard rotating wave approximation (RWA), which only takes into account the resonant interaction between the optical field and chromophores. We denote $|1\rangle$ and $|2\rangle$ as the ground and excited states of a chromophore, with the transition $|2\rangle \rightleftharpoons |1\rangle$ resonant to the spasing plasmon mode n. In this approximation, the time dependence of the nondiagonal elements of the density matrix is $(\rho^{(p)})_{12} = \bar{\rho}_{12}^{(p)}\exp(i\omega t)$ and $(\rho^{(p)})_{21} = \bar{\rho}_{12}^{(p)*}\exp(-i\omega t)$, where $\bar{\rho}_{12}^{(p)}$ is an amplitude slowly varying in time, which defines the coherence (polarization) for the $|2\rangle \rightleftharpoons |1\rangle$ spasing transition in a pth chromophore of the gain medium.

Introducing a rate constant Γ_{12} to describe the polarization relaxation and a difference $n_{21}^{(p)} = \rho_{22}^{(p)} - \rho_{11}^{(p)}$ as the population inversion for this spasing transition, we derive an equation of motion for the nondiagonal element of the density matrix as

$$\dot{\bar{\rho}}_{12}^{(p)} = -\left[i\left(\omega - \omega_{12}\right) + \Gamma_{12}\right]\bar{\rho}_{12}^{(p)} + ia_{0n}n_{21}^{(p)}\tilde{\Omega}_{12}^{(p)*}, \tag{1.17}$$

where

$$\tilde{\Omega}_{12}^{(p)} = -A_n \mathbf{d}_{12}^{(p)} \nabla \varphi_n(\mathbf{r}_p)/\hbar \tag{1.18}$$

is the one-plasmon Rabi frequency for the spasing transition in a pth chromophore and $\mathbf{d}_{12}^{(p)}$ is the corresponding transitional dipole element. Note that always $\mathbf{d}_{12}^{(p)}$ is either real or can be made real by a proper choice of the quantum state phases, making the Rabi frequency $\tilde{\Omega}_{12}^{(p)}$ also a real quantity.

An equation of motion for n_{21}^{p} can be found in a standard way by commutating it with $\hat{H}$ and adding the corresponding decay and excitation rates. To provide conditions for the population inversion ($n_{21}^{p} > 0$), we imply existence of a third level. For simplicity, we assume that it very rapidly decays into the excited state $|2\rangle$ of the chromophore, so its own population is negligible. It is pumped by an external source from the ground state (optically or electrically) with some rate that we will denote g. In this way, we obtain the following equation of motion:

$$\dot{n}_{21}^{(p)} = -4\mathrm{Im}\left[a_{0n}\bar{\rho}_{12}^{(p)}\tilde{\Omega}_{21}^{(p)}\right] - \gamma_2\left(1 + n_{21}^{(p)}\right) + g\left(1 - n_{21}^{(p)}\right), \tag{1.19}$$

where γ_2 is the decay rate $|2\rangle \rightarrow |1\rangle$.

The stimulated emission of the SPs is described as their excitation by the local field created by the coherent polarization of the gain medium. The corresponding equation of motion can be obtained using Hamiltonian (1.15) and adding the SP relaxation with a rate of γ_n as

$$\dot{a}_{0n} = \left[i\left(\omega - \omega_n\right) - \gamma_n\right] a_{0n} + i a_{0n} \sum_p \rho_{12}^{(p)*} \tilde{\Omega}_{12}^{(p)}. \tag{1.20}$$

As an important general remark, the system of Equations (1.17), (1.19), and (1.20) is highly nonlinear: Each of these equations contains a quadratic nonlinearity: a product of the plasmon-field amplitude a_{0n} by the density matrix element ρ_{12} or population inversion n_{21}. Altogether, this is a six-order nonlinearity. This nonlinearity is a fundamental property of the spaser equations, which makes the spaser generation always a fundamentally nonlinear process. This process involves a nonequilibrium phase transition and a spontaneous symmetry breaking: establishment of an arbitrary but sustained phase of the coherent SP oscillations.

A relevant process is spontaneous emission of SPs by a chromophore into a spasing SP mode. The corresponding rate $\gamma_2^{(p)}$ for a chromophore at a point $\mathbf{r}_p$ can be found in a standard way using the quantized field (1.10) as

$$\gamma_2^{(p)} = 2\frac{A_n^2}{\hbar\gamma_n}\left|\mathbf{d}_{12}\nabla\varphi_n(\mathbf{r}_p)\right|^2 \frac{(\Gamma_{12} + \gamma_n)^2}{(\omega_{12} - \omega_n)^2 + (\Gamma_{12} + \gamma_n)^2}. \tag{1.21}$$

As in Schawlow-Townes theory of laser-line width [68], this spontaneous emission of SPs leads to the diffusion of the phase of the spasing state. This defines width γ_s of the spasing line as

$$\gamma_s = \frac{\sum_p \left(1 + n_{21}^{(p)}\right) \gamma_2^{(p)}}{2(2N_p + 1)}. \tag{1.22}$$

This width is small for a case of developed spasing when $N_p \gg 1$. However, for $N_p \sim 1$, the predicted width may be too high because the spectral diffusion theory assumes that $\gamma_s \lesssim \gamma_n$. To take into account this limitation in a simplified way, we will interpolate to find the resulting spectral width Γ_s of the spasing line as $\Gamma_s = (\gamma_n^{-2} + \gamma_s^{-2})^{-1/2}$.

We will also examine the spaser as a bistable (logical) amplifier. One of the ways to set the spaser in such a mode is to add a saturable absorber. This is described by the same Equations (1.17), (1.18), (1.19), and (1.20) where the chromophores belonging to the absorber are not pumped by the external source directly, that is, for them in Equation (1.19) one has to set $g = 0$.

Numerical examples are given for a silver nanoshell where the core and the external dielectric have the same permittivity of $\varepsilon_d = 2$; the permittivity of silver is adopted from Reference 69. The following realistic parameters of the gain medium are used (unless indicated otherwise): $d_{12} = 1.5 \times 10^{-17}$ esu, $\hbar\Gamma_{12} = 10$ meV, $\gamma_2 = 4 \times 10^{12}\,\mathrm{s}^{-1}$ (this value takes into account the spontaneous decay into SPs), and density of the gain medium chromophores is $n_c = 2.4 \times 10^{20}\,\mathrm{cm}^{-3}$, which is realistic for dye molecules but may be somewhat high for semiconductor QDs that were proposed as the chromophores [15] and used in experiments [46]. We will assume a dipole SP mode and chromophores situated in the core of the nanoshell as shown in Figure 1.2d. This configuration is of advantage both functionally (because the region of the high local fields outside the shell is accessible for various applications) and computationally (the uniformity of the modal fields makes the summation of the chromophores trivial, thus greatly facilitating numerical procedures).

1.3.3 Equations for CW Regime

Physically, the spaser action is a result of spontaneous symmetry breaking when the phase of the coherent SP field is established from the spontaneous noise. Mathematically, the spaser is described by homogeneous differential Equations (1.17), (1.18), (1.19), and (1.20). These equations become homogeneous algebraic equations for the CW case. They always have a trivial, zero solution. However, they may also possess a nontrivial solution describing spasing. An existence condition of such a nontrivial solution is

$$(\omega_s - \omega_n + i\gamma_n)^{-1} \times \tag{1.23}$$
$$(\omega_s - \omega_{21} + i\Gamma_{12})^{-1} \sum_p \left|\tilde{\Omega}_{12}^{(p)}\right|^2 n_{21}^{(p)} = -1,$$

where ω_s is the generation (spasing) frequency. Here, the population inversion of a pth chromophore $n_{21}^{(p)}$ is explicitly expressed as

$$n_{21}^{(p)} = (g - \gamma_2) \times \left\{ g + \gamma_2 + 4N_n \left|\tilde{\Omega}_{12}^{(p)}\right|^2 / \left[(\omega_s - \omega_{21})^2 + \Gamma_{12}^2\right] \right\}^{-1}. \tag{1.24}$$

From the imaginary part of Equation (1.24) we immediately find the spasing frequency ω_s,

$$\omega_s = \left(\gamma_n \omega_{21} + \Gamma_{12}\omega_n\right) / \left(\gamma_n + \Gamma_{12}\right), \tag{1.25}$$

which generally does not coincide with either the gain transition frequency ω_{21} or the SP frequency ω_n, but is between them. Note that this is a frequency walk-off phenomenon similar to that well known in laser physics. Substituting Equation (1.25) back into Equations (1.24) and (1.25), we obtain a system of equations:

$$\frac{(\gamma_n + \Gamma_{12})^2}{\gamma_n \Gamma_{12}\left[(\omega_{21} - \omega_n)^2 + (\Gamma_{12} + \gamma_n)^2\right]} \times \sum_p \left|\tilde{\Omega}_{12}^{(p)}\right|^2 n_{21}^{(p)} = 1, \tag{1.26}$$

$$n_{21}^{(p)} = (g - \gamma_2) \times \left[g + \gamma_2 + \frac{4N_n \left|\tilde{\Omega}_{12}^{(p)}\right|^2 (\Gamma_{12} + \gamma_n)}{(\omega_{12} - \omega_n)^2 + (\Gamma_{12} + \gamma_n)^2} \right]^{-1}. \tag{1.27}$$

This system defines the stationary (for the CW generation) number of SPs per spasing mode, N_n.

Since $n_{21}^{(p)} \leq 1$, from Equations (1.26) and (1.27) we immediately obtain a necessary condition of the existence of spasing:

$$\frac{(\gamma_n + \Gamma_{12})^2}{\gamma_n \Gamma_{12}\left[(\omega_{21} - \omega_n)^2 + (\Gamma_{12} + \gamma_n)^2\right]} \sum_p \left|\tilde{\Omega}_{12}^{(p)}\right|^2 \geq 1. \tag{1.28}$$

This expression is fully consistent with Reference 15. The following order of magnitude estimate of this spasing condition has a transparent physical meaning and is of heuristic value:

$$\frac{d_{12}^2 Q N_c}{\hbar \Gamma_{12} V_n} \gtrsim 1, \tag{1.29}$$

where $Q = \omega/\gamma_n$ is the quality factor of SPs, V_n is the volume of the spasing SP mode, and N_c is the number of gain medium chromophores within this volume. Deriving this estimate, we have neglected the detuning, that is, set $\omega_{21} - \omega_n = 0$. We also used the definitions of A_n of Equation (1.10) and $\tilde{\Omega}_{12}^{(p)}$ given by Equation (1.18) and the estimate $|\nabla\varphi_n(\mathbf{r})|^2 \sim 1/V$ following from the normalization of the SP eigenmodes $\int |\nabla\varphi_n(\mathbf{r})|^2 d^3r = 1$ of Reference 41. The result of Equation (1.29) is, indeed, in agreement with Reference 15 where it was obtained in different notations.

It follows from Equation (1.29) that for the existence of spasing it is beneficial to have a high quality factor Q, a high density of the chromophores, and a large transition dipole (oscillator strength) of the chromophore transition. The small modal volume V_n (at a given number of the chromophores N_c) is beneficial for this spasing condition: Physically, it implies strong feedback in the spaser. Note that for the given density of the chromophores $n_c = N_c/V_n$, this spasing condition does not explicitly depend on the spaser size, which opens up a possibility of spasers of a very small size limited from the bottom by only the nonlocality radius $l_{nl} \sim 1$ nm. Another important property of Equation (1.29) is that it implies the quantum-mechanical nature of spasing and spaser amplification: This condition fundamentally contains the Planck constant $\hbar$ and, thus, does not have a classical counterpart. Note that in contrast to lasers, the spaser theory and Equations (1.28) and (1.29) in particular do not contain speed of light, that is, they are quasistatic.

Now we will examine the spasing condition and reduce it to a requirement for the gain medium. First, we substitute into Equation (1.28) all the definitions and assume perfect resonance between the generating SP mode and the gain medium, that is, $\omega_n = \omega_{21}$. As a result, we obtain from Equation (1.28),

$$\frac{4\pi}{3}\frac{s_n\,|\mathbf{d}_{12}|^2}{\hbar\gamma_n\Gamma_{12}\varepsilon_d s_n'}\int_V [1-\Theta(\mathbf{r})]\,|\mathbf{E}_n(\mathbf{r})|^2\,d^3r \geq 1, \tag{1.30}$$

where the integral is extended over the volume V of the system, and the Θ-function takes into account a simplifying realistic assumption that the gain medium occupies the entire space free from the core's metal. We also assume that the orientations of the transition dipoles $\mathbf{d}_{12}^{(p)}$ are random and average over them, which results in the factor of 3 in the denominator in Equation (1.30).

From Equations (1.7) or (1.9) it can be obtained that

$$\int_V [1-\Theta(\mathbf{r})]\,|\mathbf{E}_n(\mathbf{r})|^2\,d^3r = 1 - s_n. \tag{1.31}$$

Next, we give approximate expressions for the spectral parameter (1.6), which are very accurate for the realistic case of $Q \gg 1$:

$$\operatorname{Im} s(\omega) = \frac{s_n^2}{\varepsilon_d}\operatorname{Im}\varepsilon_m(\omega) = \frac{1}{Q}s_n\,(1-s_n)\,. \tag{1.32}$$

Taking into account Equations (1.31) and (1.32), we obtain from Equation (1.30) a necessary condition of spasing at a frequency ω as

$$\frac{4\pi}{3}\frac{|\mathbf{d}_{12}|^2 n_c\,[1-\mathrm{Re}\,s(\omega)]}{\hbar\Gamma_{12}\mathrm{Re}\,s(\omega)\mathrm{Im}\,\varepsilon_m(\omega)} \geq 1. \tag{1.33}$$

This condition can also be given an alternative form conventional in laser physics in the following way. For the sake of comparison, consider a continuous gain medium comprised of the same chromophores as the gain shell of the spaser. Its gain g (it is the linear gain whose dimensionality is cm^{-1}) is given by a standard expression

$$g = \frac{4\pi}{3}\frac{\omega}{c}\frac{\sqrt{\varepsilon_d}\,|\mathbf{d}_{12}|^2 n_c}{\hbar\Gamma_{12}}. \tag{1.34}$$

Taking this into account, from Equation (1.33), we obtain the spasing criterion in terms of the gain as

$$g \geq g_{th},\, g_{th} = \frac{\omega}{c\sqrt{\varepsilon_d}}\frac{\mathrm{Re}\,s(\omega)}{1-\mathrm{Re}\,s(\omega)}\mathrm{Im}\,\varepsilon_m(\omega) \tag{1.35}$$

where g_{th} has a meaning of the threshold gain needed for spasing. Importantly, this gain depends only on the dielectric properties of the system and spasing frequency but not on the geometry of the system or the distribution of the local fields of the spasing mode (hot spots, etc.) explicitly. However, note that the system's geometry (along with the permittivities) does define the spasing frequency.

In Figures 1.3a and 1.3b, we illustrate the analytical expression (1.35) for gold and silver, correspondingly, embedded in a dielectric with $\varepsilon_d = 2$ (simulating a

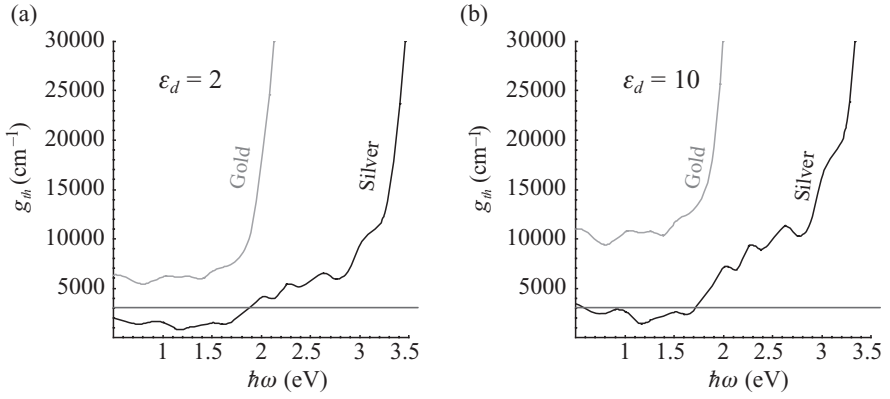

FIGURE 1.3 Threshold gain for spasing g_{th} for silver and gold, as indicated in the graphs, as a function of the spasing frequency ω. The red line separates the area $g_{th} < 3 \times 10^3\ \mathrm{cm}^{-1}$, which can relatively easily be achieved with direct band-gap semiconductors (DBGSs). The real part of the gain medium permittivity is denoted in the corresponding panels as ε_d.

light glass) and $\varepsilon_d = 10$ (simulating a semiconductor), correspondingly. These are computed from Equation (1.35) assuming that the metal core is embedded into the gain medium with the real part of the dielectric function equal to ε_d. As we see from Figure 1.3, the spasing is possible for silver in the near-IR communication range and the adjacent red portion of the visible spectrum for a gain $g < 3000\,\mathrm{cm}^{-1}$ (regions below the red line in Figure 1.3), which is realistically achievable with direct band-gap semiconductors (DBGSs).

1.3.4 Spaser operation in CW Mode

The "spasing curve" (a counterpart of the light–light curve, or L–L curve, for lasers), which is the dependence of the coherent SP population N_n on the excitation rate g, obtained by solving Equations (1.26) and (1.27), is shown in Figure 1.4a for four types of the silver nanoshells with the frequencies of the spasing dipole modes as indicated, which are in the range from near-IR ($\hbar\omega_s = 1.2$ eV) to mid-visible ($\hbar\omega_s = 2.2$ eV). In all cases, there is a pronounced threshold of the spasing at an excitation rate $g_{th} \sim 10^{12}\,\mathrm{s}^{-1}$. Soon above the threshold, the dependence $N_n(g)$ becomes linear, which means that every quantum of excitation added to the active medium with a high probability is stimulated to be emitted as an SP, adding to the coherent SP population, or is dissipated to the heat due to the metal loss with a constant branching ratio between these two processes.

While this is similar to conventional lasers, there is a dramatic difference for the spaser. In lasers, a similar relative rate of the stimulated emission is achieved at a photon population of $\sim 10^{18} - 10^{20}$, while in the spaser the SP population is $N_n \lesssim 100$. This is due to the much stronger feedback in spasers because of the much smaller modal volume V_n—see discussion of Equation (1.29). The shape of the spasing curves of Figure 1.4a (the well-pronounced threshold with the linear dependence almost immediately above the threshold) is in a qualitative agreement with the experiment [27].

The population inversion number n_{21} as a function of the excitation rate g is displayed in Figure 1.4b for the same set of frequencies (and with the same color coding) as in panel (a). Before the spasing threshold, n_{21} increases with g to become positive with the onset of the population inversion just before the spasing threshold. For higher g, after the spasing threshold is exceeded, the inversion n_{21} becomes constant (the inversion clamping). The clamped levels of the inversion are very low, $n_{21} \sim 0.01$, which again is due to the very strong feedback in the spaser.

The spectral width Γ_s of the spaser generation is due to the phase diffusion of the quantum SP state caused by the noise of the spontaneous emission of the SPs into the spasing mode, as described by Equation (1.22). This width is displayed in Figure 1.4c as a function of the pumping rate g. At the threshold, Γ_s is that of the SP line γ_n but for stronger pumping, as the SPs accumulate in the spasing mode, it decreases $\propto N_n^{-1}$, as given by Equation (1.22). This decrease of Γ_s reflects the higher coherence of the spasing state with the increased number of SP quanta and, correspondingly, lower quantum fluctuations. As we have already mentioned, this is similar to the lasers as described by the Schawlow–Townes theory [68].

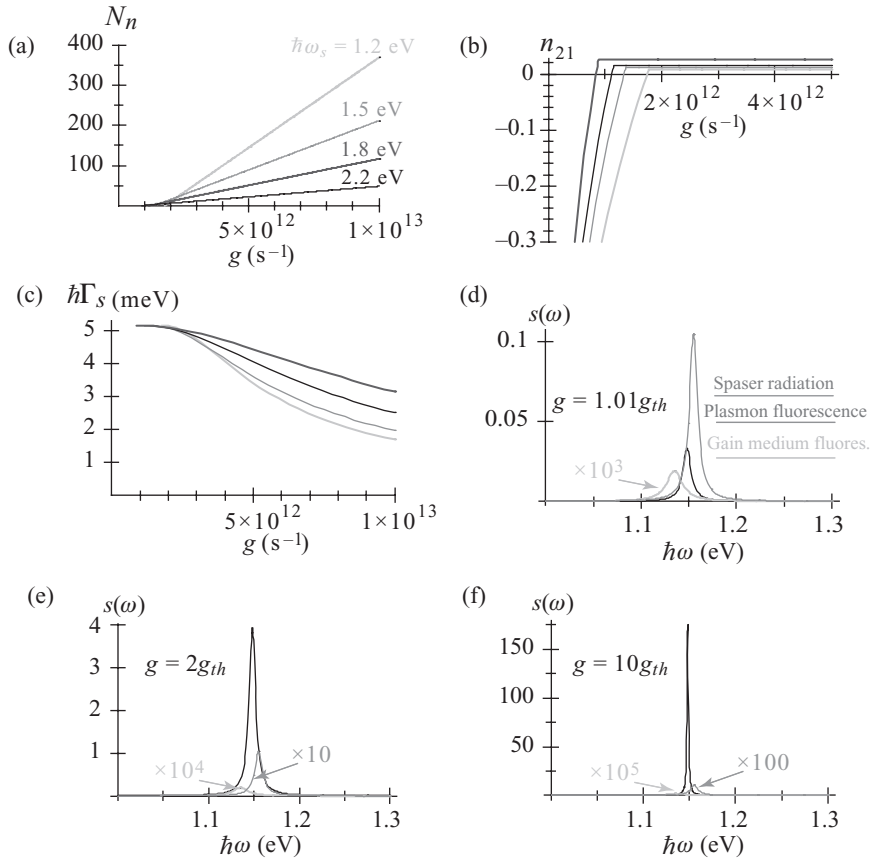

FIGURE 1.4 Spaser SP population and spectral characteristics in the stationary state. The computations are done for a silver nanoshell with the external radius $R_2 = 12$ nm; the detuning of the gain medium from the spasing SP mode is $\hbar(\omega_{21} - \omega_n) = -0.02$ eV. The other parameters are indicated in the text in Section 1.3.2. (a) Number N_n of plasmons per spasing mode as a function of the excitation rate g (per one chromophore of the gain medium). Computations are done for the dipole eigenmode with the spasing frequencies ω_s as indicated, which were chosen by the corresponding adjustment of the nanoshell aspect ratio. (b) Population inversion n_{12} as a function of the pumping rate g. The color coding of the lines is the same as in panel (a). (c) The spectral width Γ_s of the spasing line (expressed as $\hbar\Gamma_s$ in meV) as a function of the pumping rate g. The color coding of the lines is the same as in panel (a). (d)–(f) Spectra of the spaser for the pumping rates g expressed in the units of the threshold rate g_{th}, as indicated in the panels. The curves are color-coded and scaled as indicated.

The developed spasing in a dipole SP mode will show itself in the far field as an anomalously narrow and intense radiation line. The shape and intensity of this line in relation to the lines of the spontaneous fluorescence of the isolated gain medium and its SP-enhanced fluorescence line in the spaser is illustrated in Figures 1.4d–1.4f. Note that for the system under consideration, there is a 20 meV red shift of the gain medium fluorescence with respect to the SP line center. It is chosen

so as to illustrate the spectral walk-off of the spaser line. For 1% in the excitation rate above the threshold of the spasing [panel (d)], a broad spasing line (red color) appears comparable in intensity to the SP-enhanced spontaneous fluorescence line (blue color). The width of this spasing line is approximately the same as of the fluorescence, but its position is shifted appreciably (spectral walk-off) toward the isolated gain medium line (green color). For the pumping twice more intense [panel (e)], the spaser-line radiation dominates, but its width is still close to that of the SP line due to significant quantum fluctuations of the spasing state phase. Only when the pumping rate is an order of magnitude above the threshold, the spaser line strongly narrows [panel (f)], and it also completely dominates the spectrum of the radiation. This is a regime of small quantum fluctuations, which is desired in applications.

These results in the spasing region are different in the most dramatic way from previous phenomenological models [43, 51]. For instance, in a "toy model" [51], the width of the resonance line tends to zero at the threshold of spasing and then broadens up again. This distinction of the present theory is due to the nature of the spasing as a spontaneous symmetry breaking (nonequilibrium phase transition with a randomly established but sustained phase) leading to the establishment of a coherent SP state. This nonequilibrium phase transition to spasing and the spasing itself are contained in the present theory due to the fact that the fundamental equations of the spasing (1.17), (1.19), and (1.20) are nonlinear, as we have already discussed above in conjunction with these equations—see the text after Equation (1.20). The previous publications on gain compensation by loss [43,51,53] based on linear electrodynamic equations do not contain spasing. Therefore, they are not applicable in the region of the complete loss compensation and spasing.

1.3.5 Spaser as Ultrafast Quantum Nanoamplifier

As we have already mentioned in Section 1.1, a fundamental and formidable problem is that, in contrast to the conventional lasers and amplifiers in quantum electronics, the spaser has an inherent feedback, which is due to the localization of SP modes, which fundamentally cannot be removed. Such a spaser will develop generation and accumulation of the macroscopic number of coherent SPs in the spasing mode. This leads to the population inversion clamping in the CW regime at a very low level—cf. Figure 1.4b. This CW regime corresponds to the net amplification equals zero, which means that the gain exactly compensates the loss, whose condition is expressed by Equation (1.26). This is a consequence of the nonlinear gain saturation. This holds for any stable CW generator in the CW regime (including any spaser or laser) and precludes using them as amplifiers.

There are several ways to set a spaser as a quantum amplifier. One of them is to reduce the feedback, that is, to allow some or most of the SP energy in the spaser to escape from the active region, so the spaser will not generate in the region of amplification. Such a root has successfully been employed to build an SPP plasmonic amplifier on the long-range plasmon polaritons [64]. A similar root for the SP spasers would be to allow some optical energy to escape either by a near-field coupling or

by a radiative coupling to far-field radiation. The near-field coupling approach is promising for building integrated active circuits of the spasers.

Following Reference 18, we consider here two distinct approaches for setting the spasers as quantum nanoamplifiers. The first is a transient regime based on the fact that the establishment of the CW regime and the consequent inversion clamping and the total gain vanishing require some time that is determined mainly by the rate of the quantum feedback and depends also on the relaxation rates of the SPs and the gain medium. After the population inversion is created by the onset of pumping and before the spasing spontaneously develops, as we show below in this section, there is a time interval of approximately 250 fs, during which the spaser provides usable (and as predicted, quite high) amplification—see Section 1.3.6 below.

The second approach to set the spaser as a logical quantum nanoamplifier is a bistable regime that is achieved by introducing a saturable absorber into the active region, which prevents the spontaneous spasing. Then injection of a certain above-threshold number of SP quanta will saturate the absorber and initiate the spasing. Such a bistable quantum amplifier will be considered below in Section 1.3.6.1.

The temporal behavior of the spaser has been found by direct numerical solution of Equations (1.17), (1.18), (1.19), and (1.20). This solution is facilitated by the fact that in the model under consideration all the chromophores experience the same local field inside the nanoshell, and there are only two types of such chromophores: belonging to the gain medium and the saturable absorber, if it is present.

1.3.6 Monostable Spaser as a Nanoamplifier in Transient Regime

Here we consider a monostable spaser in a transient regime. This implies that no saturable absorber is present. We will consider two pumping regimes: stationary and pulse.

Starting with the stationary regime, we assume that the pumping at a rate (per one chromophore) of $g = 5 \times 10^{12}\,\mathrm{s}^{-1}$ starts at a moment of time $t = 0$ and stays constant after that. Immediately at $t = 0$, a certain number of SPs are injected into the spaser. We are interested in its temporal dynamics from this moment on.

The dynamical behavior of the spaser under this pumping regime is illustrated in Figures 1.5a and 1.5b. As we see, the spaser, which starts from an arbitrary initial population N_n, rather rapidly, within a few hundred femtoseconds approaches the same stationary ("logical") level. At this level, an SP population of $N_n = 67$ is established, while the inversion is clamped at a low level of $n_{21} = 0.02$. On the way to this stationary state, the spaser experiences relaxation oscillations in both the SP numbers and inversion, which have a trend to oscillate out of phase [compare panels (a) and (b)]. This temporal dynamics of the spaser is quite complicated and highly nonlinear (unharmonic). It is controlled not by a single relaxation time but by a set of relaxation rates. Clearly, among these are the energy transfer rate from the gain medium to the SPs and the relaxation rates of the SPs and the chromophores.

In this mode, the main effect of the initial injection of the SPs (described theoretically as different initial values of N_n) is in the interval of time required for the spaser to reach the final (CW) state. For very small N_n, which in practice can be supplied by

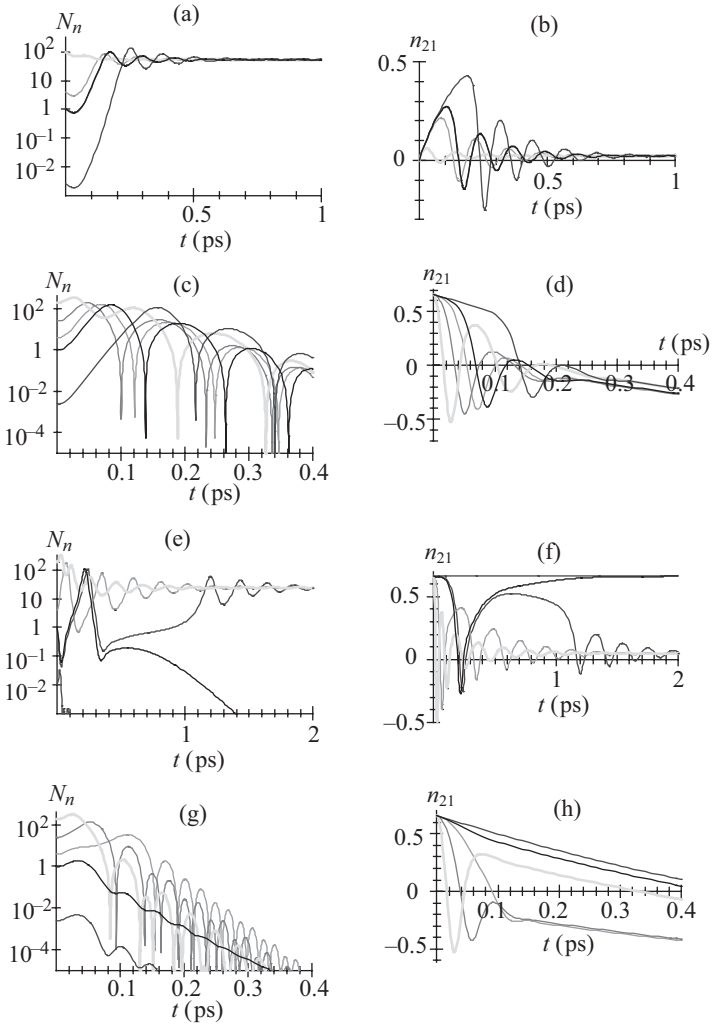

FIGURE 1.5 Ultrafast dynamics of spaser. (a) For monostable spaser (without a saturable absorber), dependence of SP population in the spasing mode N_n on time t. The spaser is stationary pumped at a rate of $g = 5 \times 10^{12}\ \mathrm{s}^{-1}$. The color-coded curves correspond to the initial conditions with the different initial SP populations, as shown in the graph. (b) The same as (a) but for the temporal behavior of the population inversion n_{21}. (c) Dynamics of a monostable spaser (no saturable absorber) with the pulse pumping described as the initial inversion $n_{21} = 0.65$. Coherent SP population N_n is displayed as a function of time t. Different initial populations are indicated by color-coded curves. (d) The same as (c) but for the corresponding population inversion n_{21}. (e) The same as (a) but for bistable spaser with the saturable absorber in concentration $n_a = 0.66n_c$. (f) The same as (b) but for the bistable spaser. (g) The same as (e) but for the pulse pumping with the initial inversion $n_{21} = 0.65$. (h) The same as (g) but for the corresponding population inversion n_{21}.

the noise of the spontaneous SP emission into the mode, this time is approximately 250 fs (cf. the corresponding SP relaxation time is less than 50 fs). In contrast, for the initial values of $N_n = 1 - 5$, this time shortens to 150 fs.

Now consider the second regime: pulse pumping. The gain medium population of the spaser is inverted at $t = 0$ to saturation with a short (much shorter than 100 fs) pump pulse. Simultaneously, at $t = 0$, some number of plasmons are injected (say, by an external nanoplasmonic circuitry). In response, the spaser should produce an amplified pulse of the SP excitation. Such a function of the spaser is illustrated in Figures 1.5c and 1.5d.

As we see from panel (c), independent of the initial number of SPs, the spaser always generates a series of SP pulses, of which only the first pulse is large (at or above the logical level of $N_n \sim 100$). (An exception is a case of little practical importance when the initial $N_n = 120$ exceeds this logical level, when two large pulses are produced.) The underlying mechanism of such a response is the rapid depletion of the inversion seen in panel (d), where energy is dissipated in the metal of the spaser. The characteristic duration of the SP pulse ~ 100 fs is defined by this depletion, controlled by the energy transfer and SP relaxation rates. This time is much shorter than the spontaneous decay time of the gain medium. This acceleration is due to the stimulated emission of the SPs into the spasing mode (which can be called a "stimulated Purcell effect"). There is also a pronounced trend: The lower is the initial SP population N_n, the later the spaser produces the amplified pulse. In a sense, this spaser functions as a pulse-amplitude to time-delay converter.

Now let us consider a bistable spaser as a quantum threshold (or logical) nanoamplifier. Such a spaser contains a saturable absorber mixed with the gain medium with parameters indicated at the end of Section 1.3.2 and the concentration of the saturable absorber $n_a = 0.66n_c$. This case of a bistable spaser amplifier is of particular interest because in this regime the spaser comes as close as possible in its functioning to the semiconductor-based (mostly MOSFET-based) digital nanoamplifiers. As in the previous section, we will consider two cases: stationary and short-pulse pumping.

We again start with the case of the stationary pumping at a rate of $g = 5 \times 10^{12}\ \mathrm{s}^{-1}$. We show in Figures 1.5e and 1.5f the dynamics of such a spaser. For a small initial population $N_n = 5 \times 10^{-3}$ simulating the spontaneous noise, the spaser is rapidly (faster than in 50 fs) relaxing to the zero population [panel (e)], while its gain medium population is equally rapidly approaching a high level [panel (f)] $n_{21} = 0.65$ that is defined by the competition of the pumping and the enhanced decay into the SP mode (the purple curves). This level is so high because the spasing SP mode population vanishes and the stimulated emission is absent. After reaching this stable state (which one can call, say, "logical zero"), the spaser stays in it indefinitely long despite the continuing pumping.

In contrast, for initial values N_n of the SP population large enough (for instance, for $N_n = 5$, as shown by the blue curves in Figs. 1.5e and 1.5f), the spaser tends to the "logical one" state where the stationary SP population reaches the value of $N_n \approx 60$. Due to the relaxation oscillations, it actually exceeds this level within a short time of $\lesssim 100$ fs after the seeding with the initial SPs. As the SP population N_n

reaches its stationary (CW) level, the gain medium inversion n_{21} is clamped down at a low level of a few percent, as typical for the CW regime of the spaser. This "logical one" state also persists indefinitely, as long as the inversion is supported by the pumping.

There is a critical curve (separatrix) that divides the two stable dynamics types (leading to the logical levels of zero and one). For the present set of parameters this separatrix starts with the initial population of $N_n \approx 1$. For a value of the initial N_n slightly below 1, the SP population N_n experiences a slow (hundreds of femtoseconds in time) relaxation oscillation but eventually relaxes to zero (Fig. 1.5e, black curve), while the corresponding chromophore population inversion n_{21} relaxes to the high value $n_{21} = 0.65$ [panel (f), black curve]. In contrast, for a value of N_n slightly higher than 1 [light blue curves in panels (e) and (f)], the dynamics is initially close to the separatrix but eventually the initial slow dynamics tends to the high SP population and low chromophore inversion through a series of the relaxation oscillations. The dynamics close to the separatrix is characterized by a wide range of oscillation times due to its highly nonlinear character. The initial dynamics is slowest (the "decision stage" of the bistable spaser that lasts $\gtrsim 1$ ps). The "decision time" is diverging infinitesimally close to the separatrix, as is characteristic of any threshold (logical) amplifier.

The gain (amplification coefficient) of the spaser as a logical amplifier is the ratio of the high CW level to the threshold level of the SP population N_n. For this specific spaser with the chosen set of parameters, this gain is ≈ 60, which is more than sufficient for the digital information processing. Thus this spaser can make a high gain, ~ 10 THz bandwidth logical amplifier or dynamical memory cell with excellent prospects of applications.

The last but not the least regime to consider is that of the pulse pumping in the bistable spaser. In this case, the population inversion ($n_{21} = 0.65$) is created by a short pulse at $t = 0$ and simultaneously initial SP population N_n is created. Both are simulated as the initial conditions in Equations (1.17), (1.18), (1.19), and (1.20). The corresponding results are displayed in Figures 1.5g and 1.5h.

When the initial SP population exceeds the critical one of $N_n = 1$ (the blue, green, and red curves), the spaser responds with generating a short (duration less than 100 fs) pulse of the SP population (and the corresponding local fields) within a time $\lesssim 100$ fs [panel (g)]. Simultaneously, the inversion is rapidly (within ~ 100 fs) exhausted [panel (h)].

In contrast, when the initial SP population N_n is less than the critical one (i.e., $N_n < 1$ in this specific case), the spaser rapidly (within a time $\lesssim 100$ fs) relaxes as $N_n \to 0$ through a series of relaxation oscillations—see the black and magenta curves in Figure 1.5g. The corresponding inversion decays in this case almost exponentially with a characteristic time ~ 1 ps determined by the enhanced energy transfer to the SP mode in the metal—see the corresponding curves in panel (h). Note that the SP population decays faster when the spaser is above the generation threshold due to the stimulated SP emission leading to the higher local fields and enhanced relaxation.

1.4 COMPENSATION OF LOSS BY GAIN AND SPASING

1.4.1 Introduction to Loss Compensation by Gain

Here, we will mostly follow References 19 and 20. A problem for many applications of plasmonics and metamaterials is posed by losses inherent in the interaction of light with metals. There are several ways to bypass, mitigate, or overcome the detrimental effects of these losses, which we briefly discuss below:

(i) The most common approach consists in employing effects where the losses are not fundamentally damaging such as SPP propagation used in sensing [11], ultramicroscopy [70,71], and solar energy conversion [72]. For realistic losses, there are other effects and applications that are not prohibitively suppressed by the losses and are useful, in particular, sensing based on SP resonances and surface-enhanced Raman scattering (SERS) [2, 11, 73–75].

(ii) Another promising idea is to use superconducting plasmonics to dramatically reduce losses [76–80]. However, this is only applicable for frequencies below the superconducting gaps, that is, in the terahertz region.

(iii) Yet another proposed direction is using highly doped semiconductors where the ohmic losses can be significantly lower due to much lower free carrier concentrations [81]. However, a problem with this approach may lie in the fact that the usefulness of plasmonic modes depends not on the loss *per se* but on the quality factor Q, which for doped semiconductors may not be higher than for the plasmonic metals.

(iv) One of the alternative approaches to low-loss plasmonic metamaterials is based on our idea of the spaser: It is using a gain to compensate the dielectric (ohmic) losses [82, 83]. In this case the gain medium is included into the metamaterials. It surrounds the metal plasmonic component in the same manner as in the spasers. The idea is that the gain will provide quantum amplification compensating the loss in the metamaterials, which is quite analogous to the spaser.

We will consider the theory of the loss compensation in the plasmonic metamaterials containing gain [19,20]. Below we show analytically that the full compensation or overcompensation of the optical loss in a dense resonant gain metamaterial leads to an instability that is resolved by its spasing (i.e., by becoming a generating spaser). We further show analytically that the conditions of the complete loss compensation by gain and the threshold condition of spasing—see Equations (1.33) and (1.35)—are identical. Thus the full compensation (overcompensation) of the loss by gain in such a metamaterial will cause spasing. This spasing limits (clamps) the gain—see Section 1.3.4—and, consequently, inhibits the complete loss compensation (overcompensation) at any frequency.

1.4.2 Permittivity of Nanoplasmonic Metamaterial

We consider, for certainty, an isotropic and uniform metamaterial that, by definition, in a range of frequencies ω can be described by the effective permittivity $\bar{\varepsilon}(\omega)$ and permeability $\bar{\mu}(\omega)$. We will concentrate below on the loss compensation for the

optical electric responses; Similar consideration for the optical magnetic responses is straightforward. Our theory is applicable for the true 3d metamaterials whose size is much greater than the wavelength λ (ideally, an infinite metamaterial).

Consider a small slab of such a metamaterial with sizes much greater that the unit cell but much smaller than λ. Such a piece is a metamaterial itself. Let us subject this metamaterial to a uniform electric field $\mathbf{E}(\omega) = -\nabla\phi(\mathbf{r}, \omega)$ oscillating with frequency ω. Note that $\mathbf{E}(\omega)$ is the amplitude of the macroscopic electric field inside the metamaterial. A true periodic metamaterial is a crystal where the eigenmodes are Bloch states [84]. In such a state, the field magnitude is periodic on the lattice in accord with the Bloch theorem. Consequently, the influx and outflow of energy balance each other. Thus, selecting a metamaterial slab instead of an infinite crystal will not affect the loss and its compensation.

We will denote the local field at a point $\mathbf{r}$ inside this metamaterial as $\mathbf{e}(\mathbf{r}, \omega) = -\nabla\varphi(\mathbf{r}, \omega)$. We assume standard boundary conditions

$$\varphi(\mathbf{r}, \omega) = \phi(\mathbf{r}, \omega), \tag{1.36}$$

for $\mathbf{r}$ belonging to the surface S of the slab under consideration.

To present our results in a closed form, we first derive a homogenization formula used in Reference 85 (see also references cited therein). By definition, the electric displacement in the volume V of the metamaterial is given by a formula

$$\mathbf{D}(\mathbf{r}, \omega) = \frac{1}{V}\int_V \varepsilon(\mathbf{r}, \omega)\mathbf{e}(\mathbf{r}, \omega)dV, \tag{1.37}$$

where $\varepsilon(\mathbf{r}, \omega)$ is a position-dependent permittivity. This can be identically expressed (by multiplying and dividing by the conjugate of the macroscopic field E^*) and, using the Gauss theorem, transformed to a surface integral as

$$D = \frac{1}{VE^*(\omega)}\int_V \mathbf{E}^*(\omega)\varepsilon(\mathbf{r}, \omega)\mathbf{e}(\mathbf{r}, \omega)dV = \frac{1}{VE^*(\omega)}\int_S \phi^*(\mathbf{r}, \omega)\varepsilon(\mathbf{r}, \omega)\mathbf{e}(\mathbf{r}, \omega)d\mathbf{S}, \tag{1.38}$$

where we took into account the Maxwell continuity equation $\nabla[\varepsilon(\mathbf{r}, \omega)\mathbf{e}(\mathbf{r}, \omega)] = 0$. Now, using the boundary conditions of Equation (1.36), we can transform it back to the volume integral as

$$D = \frac{1}{VE^*(\omega)}\int_S \varphi^*(\mathbf{r})\varepsilon(\mathbf{r}, \omega)\mathbf{e}(\mathbf{r}, \omega)d\mathbf{S} = \frac{1}{VE^*(\omega)}\int_V \varepsilon(\mathbf{r}, \omega)\left|\mathbf{e}(\mathbf{r}, \omega)\right|^2 dV. \tag{1.39}$$

From the last equality, we obtain the required homogenization formula as an expression for the effective permittivity of the metamaterial:

$$\bar{\varepsilon}(\omega) = \frac{1}{V\,|E(\omega)|^2}\int_V \varepsilon(\mathbf{r},\omega)\,|\mathbf{e}(\mathbf{r},\omega)|^2\,dV. \tag{1.40}$$

1.4.3 Plasmonic Eigenmodes and Effective Resonant Permittivity of Metamaterials

This piece of the metamaterial with the total size $R \ll \lambda$ can be treated in the quasistatic approximation. The local field inside the nanostructured volume V of the metamaterial is given by the eigenmode expansion [41, 66, 86]

$$\mathbf{e}(\mathbf{r},\omega) = \mathbf{E}(\omega) - \sum_n \frac{a_n}{s(\omega)-s_n}\mathbf{E}_n(\mathbf{r}), \tag{1.41}$$

$$a_n = \mathbf{E}(\omega)\int_V \theta(\mathbf{r})\mathbf{E}_n(\mathbf{r})dV,$$

where we remind that $\mathbf{E}(\omega)$ is the macroscopic field. In the resonance, $\omega = \omega_n$, only one term at the pole in Equation (1.41) dominates, and it becomes

$$\mathbf{e}(\mathbf{r},\omega) = \mathbf{E}(\omega) + i\frac{a_n}{\operatorname{Im} s(\omega_n)}\mathbf{E}_n(\mathbf{r}). \tag{1.42}$$

The first term in this equation corresponds to the mean (macroscopic) field and the second one describes the deviations of the local field from the mean field containing contributions of the hot spots [87]. The mean root square ratio of the second term (local field) to the first (mean field) is estimated as

$$\sim \frac{f}{\operatorname{Im} s(\omega_n)} = \frac{fQ}{s_n(1-s_n)}, \tag{1.43}$$

where we took into account an estimate $E_n \sim V^{-1/2}$, which follows from the eigenmode field normalization $\int_V |\mathbf{E}_n|^2 dV = 1$, and

$$f = \frac{1}{V}\int_V \theta(\mathrm{r})dV, \tag{1.44}$$

where f is the metal fill factor of the system and Q is the plasmonic quality factor. Deriving expression (1.43), we have also taken into account an equality $\operatorname{Im} s(\omega_n) = s_n(1-s_n)/Q$, which is valid in the assumed limit of the high quality factor, $Q \gg 1$ (see the next paragraph).

For a good plasmonic metal $Q \gg 1$. For most metal-containing metamaterials, the metal fill factor is not small, typically $f \gtrsim 0.5$. The eigenvalues s_n are limited [12, 41], $1 > s_n > 0$. Thus, it is very realistic to assume the following condition:

$$\frac{fQ}{s_n(1-s_n)} \gg 1. \tag{1.45}$$

If so, the second (local) term of the field (1.42) dominates and, with a good precision, the local field is approximately the eigenmode's field:

$$\mathbf{e}(\mathbf{r},\omega) = i\frac{a_n}{\operatorname{Im} s(\omega_n)}\mathbf{E}_n(\mathbf{r}). \tag{1.46}$$

Substituting this into Equation (1.40), we obtain a homogenization formula

$$\bar{\varepsilon}(\omega) = b_n \int_V \varepsilon(\mathbf{r},\omega)\,[\mathbf{E}_n(\mathbf{r})]^2\,dV, \tag{1.47}$$

where $b_n > 0$ is a real positive coefficient whose specific value is

$$b_n = \frac{1}{3V}\left(\frac{Q\int_V \theta(\mathbf{r})\mathbf{E}_n(\mathbf{r})dV}{s_n\,(1-s_n)}\right)^2. \tag{1.48}$$

Using Equation (1.47), it is straightforward to show that the effective permittivity (1.47) simplifies exactly to

$$\bar{\varepsilon}(\omega) = b_n\left[s_n\varepsilon_m(\omega) + (1-s_n)\varepsilon_h(\omega)\right]. \tag{1.49}$$

1.4.4 Conditions of Loss Compensation by Gain and Spasing

In the case of full inversion (maximum gain) and in exact resonance, the host medium permittivity acquires the imaginary part describing the stimulated emission as given by the standard expression

$$\varepsilon_h(\omega) = \varepsilon_d - i\frac{4\pi}{3}\frac{|\mathbf{d}_{12}|^2\,n_c}{\hbar\Gamma_{12}}, \tag{1.50}$$

where $\varepsilon_d = \operatorname{Re}\varepsilon_h$, $\mathbf{d}_{12}$ is a dipole matrix element of the gain transition in a chromophore center of the gain medium, Γ_{12} is a spectral width of this transition, and n_c is the concentration of these centers (these notations are consistent with those used above in Sections 1.3.2–1.3.6.1). Note that if the inversion is not maximum, then this and subsequent equations are still applicable if one sets as the chromophore concentration n_c the inversion density: $n_c = n_2 - n_1$, where n_2 and n_1 are the concentrations of the chromophore centers of the gain medium in the upper and lower states of the gain transition, respectively.

The condition for the full electric loss compensation in the metamaterial and amplification (overcompensation) at the resonant frequency $\omega = \omega_n$ is

$$\mathrm{Im}\,\bar{\varepsilon}(\omega) \leq 0. \tag{1.51}$$

Taking Equation (1.49) into account, this reduces to

$$s_n \mathrm{Im}\,\varepsilon_m(\omega) - \frac{4\pi}{3}\frac{|\mathbf{d}_{12}|^2 n_c(1-s_n)}{\hbar\Gamma_{12}} \leq 0. \tag{1.52}$$

Finally, taking into account that $\mathrm{Im}\,\varepsilon_m(\omega) > 0$, we obtain from Equation (1.52) the condition of the loss (over)compensation as

$$\frac{4\pi}{3}\frac{|\mathbf{d}_{12}|^2 n_c\,[1-\mathrm{Re}\,s(\omega)]}{\hbar\Gamma_{12}\mathrm{Re}\,s(\omega)\mathrm{Im}\,\varepsilon_m(\omega)} \geq 1, \tag{1.53}$$

where the strict inequality corresponds to the overcompensation and net amplification. In Equation (1.50) we have assumed nonpolarized gain transitions. If these transitions are all polarized along the excitation electric field, the concentration n_c should be multiplied by a factor of 3.

Equation (1.53) is a fundamental condition, which is precise [assuming that the requirement (1.45) is satisfied, which is very realistic for metamaterials] and general. Moreover, it is fully analytical and, actually, very simple. Remarkably, it depends only on the material characteristics and does not contain any geometric properties of the metamaterial system or the local fields. (Note that the system's geometry does affect the eigenmode frequencies and thus enters the problem implicitly.) In particular, the hot spots, which are prominent in the local fields of nanostructures [41, 87], are completely averaged out due to the integrations in Equations (1.40) and (1.47).

The condition (1.53) is completely nonrelativistic (quasistatic)—it does not contain speed of light c, which is characteristic also of the spaser. It is useful to express this condition also in terms of the total stimulated emission cross section $\sigma_e(\omega)$ (where ω is the central resonance frequency) of a chromophore of the gain medium as

$$\frac{c\sigma_e(\omega)\sqrt{\varepsilon_d}n_c\,[1-\mathrm{Re}\,s(\omega)]}{\omega\mathrm{Re}\,s(\omega)\mathrm{Im}\,\varepsilon_m(\omega)} \geq 1. \tag{1.54}$$

We see that Equation (1.53) *exactly* coincides with a spasing condition expressed by Equation (1.33). This brings us to an important conclusion: The full compensation (overcompensation) of the optical losses in a metamaterial [which is resonant and dense enough to satisfy condition (1.45)] and the spasing occur under precisely the same conditions.

We have considered above in Section 1.3.3 the conditions of spasing, which are equivalent to Equation (1.54). These are given by one of equivalent conditions of Equations (1.33), (1.35), and (1.53). It is also illustrated in Figure 1.3. We stress that

exactly the same conditions are for the full loss compensation (overcompensation) of a dense resonant plasmonic metamaterial with gain.

We would also like to point out that the criterion given by the equivalent conditions of Equations (1.33), (1.35), (1.53), and (1.54) is derived for localized SPs, which are describable in the quasistatic approximation, and is not directly applicable to the propagating SPP modes. However, we expect that very short wavelength SPPs, whose wave vector $k \lesssim l_s$, can be described by these conditions because they are, basically, quasistatic. For instance, the SPPs on a thin metal wire of radius $R \lesssim l_s$ are described by a dispersion relation [88]

$$k \approx \frac{1}{R}\left[-\frac{\varepsilon_m}{2\varepsilon_d}\left(\ln\sqrt{-\frac{4\varepsilon_m}{\varepsilon_d}} - \gamma\right)\right]^{-1/2}, \tag{1.55}$$

where $\gamma \approx 0.57721$ is the Euler constant. This relation is obviously quasistatic because it does not contain speed of light c.

1.4.5 Discussion of Spasing and Loss Compensation by Gain

This fact of the equivalence of the full loss compensation and spasing is intimately related to the general criteria of the thermodynamic stability with respect to small fluctuations of electric and magnetic fields—see Chapter IX of Reference 67:

$$\operatorname{Im}\bar{\varepsilon}(\omega) > 0, \operatorname{Im}\bar{\mu}(\omega) > 0, \tag{1.56}$$

which must be *strict* inequalities for all frequencies for electromagnetically stable systems. For systems in thermodynamic equilibrium, these conditions are automatically satisfied.

However, for the systems with gain, the conditions (1.56) can be violated, which means that such systems can be electromagnetically unstable. The first of conditions (1.56) is opposite to Equations (1.51) and (1.53). This has a transparent meaning: The electrical instability of the system is resolved by its spasing.

The significance of these stability conditions for gain systems can be elucidated by the following *gedanken* experiment. Take a small isolated piece of such a metamaterial (which is a metamaterial itself). Consider that it is excited at an optical frequency ω by a weak external optical field $\mathbf{E}$ or acquires such a field due to fluctuations (thermal or quantum). The energy density $\mathcal{E}$ of such a system is given by the Brillouin formula [67]

$$\mathcal{E} = \frac{1}{16\pi}\frac{\partial\omega\operatorname{Re}\bar{\varepsilon}}{\partial\omega}|\mathbf{E}|^2. \tag{1.57}$$

Note that for the energy of the system to be definite, it is necessary to assume that the loss is not too large, $|\operatorname{Re}\bar{\varepsilon}| \gg \operatorname{Im}\bar{\varepsilon}$. This condition is realistic for many metamaterials, including all potentially useful ones.

The internal optical energy-density loss per unit time Q (i.e., the rate of the heat-density production in the system) is [67]

$$Q = \frac{\omega}{8\pi} \mathrm{Im}\, \bar{\varepsilon}\, |\mathbf{E}|^2 . \tag{1.58}$$

Assume that the internal (ohmic) loss dominates over other loss mechanisms such as the radiative loss, which is also a realistic assumption since the ohmic loss is very large for the experimentally studied systems and the system itself is very small (the radiative loss rate is proportional to the volume of the system). In such a case of the dominating ohmic losses, we have $d\mathcal{E}/dt = Q$. Then Equations (1.57) and (1.58) can be resolved together yielding the energy $\mathcal{E}$ and electric field $|\mathbf{E}|$ of this system to evolve with time t exponentially as

$$|\mathbf{E}| \propto \sqrt{\mathcal{E}} \propto e^{-\Gamma t}, \Gamma = \omega \mathrm{Im}\, \bar{\varepsilon} / \frac{\partial(\omega \mathrm{Re}\, \bar{\varepsilon})}{\partial \omega}. \tag{1.59}$$

We are interested in a resonant case when the metamaterial possesses a resonance at some eigenfrequency $\omega_n \approx \omega$. For this to be true, the system's behavior must be plasmonic, that is, $\mathrm{Re}\, \bar{\varepsilon}(\omega) < 0$. Then the dominating contribution to $\bar{\varepsilon}$ comes from a resonant SP eigenmode n with a frequency $\omega_n \approx \omega$. In such a case, the dielectric function [41] $\bar{\varepsilon}(\omega)$ has a simple pole at $\omega = \omega_n$. As a result, $\partial(\omega \mathrm{Re}\, \bar{\varepsilon})/\partial\omega \approx \omega \partial \mathrm{Re}\, \bar{\varepsilon}/\partial\omega$ and, consequently, $\Gamma = \gamma_n$, where γ_n is the SP decay rate [12, 15]:

$$\gamma_n = \left. \frac{\mathrm{Im}\, \varepsilon_m(\omega)}{\frac{\partial \mathrm{Re}\varepsilon_m(\omega)}{\partial \omega}} \right|_{\omega = \omega_n}, \tag{1.60}$$

and the metal dielectric function ε_m is replaced by the effective permittivity $\bar{\varepsilon}$ of the metamaterial. Thus, Equation (1.59) is fully consistent with the spectral theory of SPs [12, 15].

If the losses are not very large so that the energy of the system is meaningful, the Kramers–Kronig causality requires [67] that $\partial(\omega \mathrm{Re}\, \bar{\varepsilon})/\partial\omega > 0$. Thus, $\mathrm{Im}\, \bar{\varepsilon} < 0$ in Equation (1.59) would lead to a negative decrement,

$$\Gamma < 0, \tag{1.61}$$

implying that the initial small fluctuation starts to grow exponentially in time in its field and energy, which is an instability. Such an instability is indeed not impossible: It will result in spasing that will eventually stabilize $|\mathbf{E}|$ and $\mathcal{E}$ at finite stationary (CW) levels of the spaser generation.

Note that the spasing limits (clamps) the gain and population inversion making *the net gain to be precisely zero* [18] in the stationary (CW) regime; see Section 1.3.5 and Figure 1.4b. Above the threshold of the spasing, the population inversion of the gain medium is clamped at a rather low level $n_{21} \sim 1\%$. The corresponding net amplification in the CW spasing regime is exactly zero, which is a condition for the

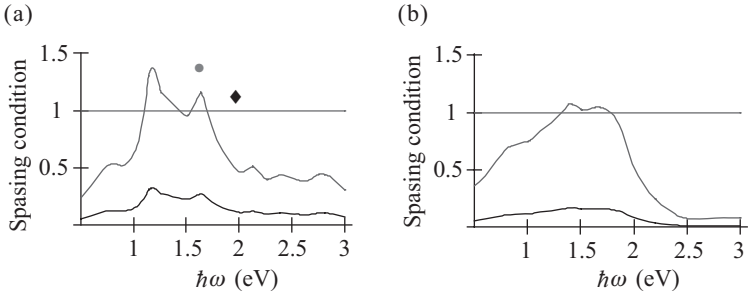

FIGURE 1.6 Spasing criterion as a function of optical frequency ω. The straight line (red line) represents the threshold for the spasing and full loss compensation, which take place for the curve segments above it. (a) Computations for silver. The chromophore concentration is $n_c = 6 \times 10^{18}\,\mathrm{cm}^{-3}$ for the lower curve (black) and $n_c = 2.9 \times 10^{19}\,\mathrm{cm}^{-3}$ for the upper curve (blue line). The black diamond shows the value of the spasing criterion for the conditions of Reference 48—see the text. (b) Computations for gold. The chromophore concentration is $n_c = 3 \times 10^{19}\,\mathrm{cm}^{-3}$ for the lower curve (black) and $n_c = 2 \times 10^{20}\,\mathrm{cm}^{-3}$ for the upper curve (blue line).

CW regime. This makes the complete loss compensation and its overcompensation impossible in a dense resonant metamaterial where the feedback is created by the internal inhomogeneities (including its periodic structure) and the facets of the system.

Because the loss (over)compensation condition (1.53), which is also the spasing condition, is geometry-independent, it is useful to illustrate it for commonly used plasmonic metals, gold and silver whose permittivity we adopt from Reference 69. For the gain medium chromophores, we will use a reasonable set of parameters: $\Gamma_{12} = 5 \times 10^{13}\,\mathrm{s}^{-1}$ and $d_{12} = 4.3 \times 10^{-18}$ esu. The results of computations are shown in Figure 1.6. (Note that this figure expresses a condition of spasing equivalent to that of Fig. 1.3.) For silver as a metal and $n_c = 6 \times 10^{18}\,\mathrm{cm}^{-3}$, the corresponding lower (black) curve in panel (a) does not reach the value of 1, implying that no full loss compensation is achieved. In contrast, for a higher but still very realistic concentration of $n_c = 2.9 \times 10^{19}\,\mathrm{cm}^{-3}$, the upper curve in Figure 1.6a does cross the threshold line in the near-IR region. Above the threshold area, there will be the instability and the onset of the spasing. As Figure 1.6b demonstrates, for gold the spasing occurs at higher, but still realistic, chromophore concentrations.

1.4.6 Discussion of Published Research on Spasing and Loss Compensations

Now let us discuss the implications of these results for the research published recently on gain metamaterials. To carry out a quantitative comparison with Reference 53, we turn to Figure 1.6a where the lower (black) curve corresponds to the nominal value of $n_c = 6 \times 10^{18}\,\mathrm{cm}^{-3}$ used in Reference 53. There is no full loss compensation and spasing. This is explained by the fact that Reference 53 uses, as a close inspection shows, the gain dipoles parallel to the field (this is equivalent to increasing n_c by a factor of 3) and the local-field enhancement [this is equivalent to increasing n_c by

a factor of $(\varepsilon_h + 2)/3$]. Because the absorption cross section of dyes is measured in the appropriate host media (liquid solvents or polymers), it already includes the Lorentz local-field factor. To compare to the results of Reference 53, we increase in our formulas the concentration n_c of the chromophores by a factor of $\varepsilon_h + 2$ to $n_c = 2.9 \times 10^{19}\,\mathrm{cm}^{-3}$, which corresponds to the upper curve in Figure 1.6a. This curve rises above the threshold line exactly in the same (infra)red region as in Reference 53.

This agreement of the threshold frequencies between our analytical theory and numerical theory [53] is not accidental: Inside the region of stability (i.e., in the absence of spasing) both theories should and do give close results, provided that the gain medium transition alignment is taken into account and the local-field factor is incorporated.

However, above the threshold (in the region of the overcompensation), there should be spasing causing the population inversion clamping and zero net gain, and not a loss compensation. To describe this effect, it is necessary to invoke Equation (1.20) for coherent SP amplitude, which is absent in Reference 53. Also fundamentally important, spasing, just like the conventional lasing, is a highly nonlinear phenomenon, which is described by nonlinear equations—see the discussion after Equation (1.20).

The complete loss compensation is stated in a recent experimental paper [89], where the system is actually a nanofilm rather than a 3d metamaterial, to which our theory would have been applicable. For the Rhodamine 800 dye used with extinction cross section [90] $\sigma = 2 \times 10^{-16}\,\mathrm{cm}^2$ at 690 nm in concentration $n_c = 1.2 \times 10^{19}\,\mathrm{cm}^{-3}$, realistically assuming $\varepsilon_d = 2.3$, for frequency $\hbar\omega = 1.7$ eV, we calculate from Equation (1.54) a point shown by the magenta solid circle in Figure 1.6a, which is significantly above the threshold. Because in such a nanostructure the local fields are very nonuniform and confined near the metal similar to the spaser, they likewise cause a feedback. The condition of Equation (1.45) is likely to be well satisfied for Reference 89. Thus, the system may spase, which would cause the clamping of inversion and loss of gain.

In contrast to these theoretical arguments, there is no evidence of spasing indicated in the experiment—see Reference 89, which can be explained by various factors. Among them, the system of Reference 89 is a gain-plasmonic nanofilm and not a true 3d material. This system is not isotropic. Also, the size of the unit cell $a \approx 280$ nm is significantly greater than the reduced wavelength $\bar{\lambda}$, which violates the quasistatic conditions and makes the possibility of homogenization and considering this system as an optical metamaterial problematic. This circumstance may lead to an appreciable spatial dispersion. It may also cause a significant radiative loss and prevent spasing for some modes.

We would also like to point out that the fact that the unit cell of the negative-refracting (or double-negative) metamaterial of Reference 89 is relatively large, $a \approx$ 280 nm, is not accidental. As follows from theoretical consideration of Reference 91, optical magnetism and, consequently, negative refraction for metals, is only possible if the minimum scale of the conductor feature (the diameter d of the nanowire) is greater than the skin depth, $d \gtrsim l_s \approx 25$ nm, which allows one to circumvent Landau–Lifshitz's limitation on the existence of optical magnetism [67,91]. Thus, a ring-type resonator structure would have a size $\gtrsim 2l_s$ (two wires forming a loop) and still the

same diameter for the hole in the center, which comes to the total of $\gtrsim 4l_s \approx 100$ nm. Leaving the same distance between the neighboring resonator wires, we arrive at an estimate of the size of the unit cell $a \gtrsim 8l_s = 200$ nm, which is, indeed, the case for Reference 89 and other negative-refraction "metamaterials" in the optical region. This makes our theory not directly applicable to them. Nevertheless, if the spasing condition (1.33) [or (1.35) or (1.54)] is satisfied, the system still may spase on the hot-spot defect modes.

In an experimental study of the lasing spaser [46], a nanofilm of PbS QDs was positioned over a 2d metamaterial consisting of an array of negative split ring resonators. When the QDs were optically pumped, the system exhibited an increase of the transmitted light intensity on the background of a strong luminescence of the QDs but apparently did not reach the lasing threshold. The polarization-dependent loss compensation was only $\sim 1\%$. Similarly, for an array of split ring resonators over a resonant quantum well, where the inverted electron–hole population was excited optically [92], the loss compensation did not exceed $\sim 8\%$. The relatively low-loss compensation in these papers may be due to random spasing and/or spontaneous or amplified spontaneous emission enhanced by this plasmonic array, which reduces the population inversion.

A dramatic example of possible random spasing is presented in Reference 48. The system studied was a Kretschmann-geometry SPP setup [93] with an added ~ 1 μm polymer film containing Rhodamine 6G dye in the $n_c = 1.2 \times 10^{19}\,\mathrm{cm}^{-3}$ concentration. When the dye was pumped, there was outcoupling of radiation in a range of angles. This was a threshold phenomenon with the threshold increasing with the Kretschmann angle. At the maximum of the pumping intensity, the widest range of the outcoupling angles was observed, and the frequency spectrum at every angle narrowed to a peak near a single frequency $\hbar\omega \approx 2.1$ eV.

These observations of Reference 48 can be explained by the spasing where the feedback is provided by the roughness of the metal. At high pumping, the localized SPs (hot spots), which possess the highest threshold, start to spase in a narrow frequency range around the maximum of the spasing criterion—the left-hand side of Equation (1.53). Because of the subwavelength size of these hot spots, the Kretschmann phase-matching condition is relaxed, and the radiation is outcoupled into a wide range of angles.

The SPPs of Reference 48 excited by the Kretschmann coupling are short-range SPPs, very close to the antisymmetric SPPs. They are localized at subwavelength distances from the surface, and their wavelength in the plane is much shorter the ω/c. Thus they can be well described by the quasistatic approximation and the present theory is applicable to them. Substituting the above given parameters of the dye and the extinction cross section $\sigma_e = 4 \times 10^{-16}\,\mathrm{cm}^2$ into Equation (1.54), we obtain a point shown by the black diamond in Figure 1.6, which is clearly above the threshold, supporting our assertion of the spasing. Likewise, the amplified spontaneous emission and possibly spasing appear to have prevented the full loss compensation in an SPP system of Reference 60.

Note that the long-range SPPs of Reference 64 are localized significantly weaker (at distances $\sim \lambda$) than those excited in Kretschmann geometry. Thus the long-range

SPPs experience a much weaker feedback, and the amplification instead of the spasing can be achieved. Generally, the long-range SPPs are fully electromagnetic (non-quasistatic) and are not describable in the present theory.

As we have already discussed in conjunction with Figure 1.3, the spasing is readily achievable with the gain medium containing common DBGSs or dyes. There have been numerous experimental observations of the spaser—see, in particular, References 27–33. Among them is a report of an SP spaser with a 7 nm gold nanosphere as its core and a laser dye in the gain medium [27], observations of the SPP spasers (also known as nanolasers) with silver as a plasmonic-core metal and DBGS as the gain medium with a 1d confinement [28, 31], a tight 2d confinement [29], and a 3d confinement [30]. There has also been a report on observation of an SPP microcylinder spaser [94]. A high-efficiency room-temperature semiconductor spaser with a DBGS InGaAS gain medium operating near 1.5 μm (i.e., in the communication near-IR range) has been reported [31].

The research and development in the area of spasers as quantum nanogenerators is very active and will undoubtedly lead to further rapid advances. The next in line is the spaser as an ultrafast nanoamplifier, which is one of the most important tasks in nanotechnology.

In contrast to this success and rapid development in the field of spasing and spasers, there has so far been a comparatively limited progress in the field of loss compensation by gain in metamaterials, which is based on the same principles of quantum amplification as the spaser. This status exists despite a significant effort in this direction and numerous theoretical publications (e.g., [53,95]). There has been so far a single, not yet confirmed independent, observation of the full loss compensation in a plasmonic metamaterial with gain [89].

In large periodic metamaterials, plasmonic modes are generally propagating waves (SPPs) that satisfy the Bloch theorem [84] and are characterized by quasi-wave vector $\mathbf{k}$. These are propagating waves except for the band edges where $\mathbf{ka} = \pm\pi$, where $\mathbf{a}$ is the lattice vector. At the band edges, the group velocity v_g of these modes is zero, and these modes are localized, that is, they are SPs. Their wave function is periodic with period $2a$, which may be understood as a result of the Bragg reflection from the crystallographic planes. Within this $2a$ period, these band-edge modes can, indeed, be treated quasistatically because $2a \ll l_s, \bar{\lambda}$. If any of the band-edge frequencies is within the range of compensation [where the condition (1.33) [or (1.35)] is satisfied], the system will spase. The same is true for nonpropagating modes whose frequencies are in the band gap. In fact, at the band edge or in the band gap, a metamaterial with gain is similar to a DFB laser [96]—see also the next paragraph.

There has been a recent experimental observation [33] of an electrically pumped DFB nanolaser (spaser) working in the communication frequency range at room temperature. This spaser generates on a stop-band (nonpropagating) plasmonic mode, that is, a mode with frequency within the band gap. The system is a 1d plasmonic-crystal metamaterial with gain, containing a Bragg grating. There is a strong coupling between the unit cells typical for DFB lasers. Because of the suppression of the spontaneous emission and the strong coupling between the unit cells leading to efficient feedback, this spaser has a significantly lower threshold, narrow spectral

line, and higher efficiency of the generation than the ones working on SPP reflection from the edges. This observation is in full agreement with our theoretical arguments [97] and in direct contradiction with the contention of Reference 98 that coupling between the unit cells increases the spasing threshold.

Moreover, the SPPs, which are at the band edge or in the band gap, will not just be localized. Due to unavoidable disorder caused by fabrication defects in metamaterials, there will be scattering of the SPPs from these defects. Close to the band edge, the group velocity becomes small, $v_g \to 0$. Because the scattering cross section of any wave is $\propto v_g^{-2}$, the corresponding SPPs experience Anderson localization [99]. Also, there will always be SPs nanolocalized at the defects of the metamaterial, whose local fields are hot spots [87, 100, 101]. Each of such hot spots within the bandwidth of conditions (1.33) or (1.35) will be a generating spaser, which clamps the inversion and precludes the full loss compensation.

Note that for a 2d metamaterial (metasurface), the amplification of the spontaneous emission and spasing may occur in SPP modes propagating *in plane* of the structure, unlike the signal that propagates normally to it as in Reference 89.

ACKNOWLEDGMENTS

This work was supported by Grant No. DEFG02-01ER15213 from the Chemical Sciences, Biosciences and Geosciences Division and by Grant No. DE-FG02-11ER46789 from the Materials Sciences and Engineering Division of the Office of the Basic Energy Sciences, Office of Science, U.S. Department of Energy, and by a grant from the U.S. Israel Binational Science Foundation.

REFERENCES

1. Atwater HA (2007) The promise of plasmonics. *Sci. Am.* 296: 56–63.
2. Anker JN, Hall WP, Lyandres O, Shah NC, Zhao J, Duyne RPV (2008) Biosensing with plasmonic nanosensors. *Nat. Mater.* 7: 442–453.
3. Novotny L, Hecht B (2006) *Principles of Nano-Optics*. Cambridge, NY: Cambridge University Press.
4. Israel A, Mrejen M, Lovsky Y, Polhan M, Maier S, Lewis A (2007) Near-field imaging probes electromagnetic waves. *Laser Focus World* 43: 99–102.
5. Tang L, Kocabas SE, Latif S, Okyay AK, Ly-Gagnon DS, Saraswat KC, Miller DAB (2008) Nanometre-scale germanium photodetector enhanced by a near-infrared dipole antenna. *Nat. Photonics* 2: 226–229.
6. Challener WA, Peng C, Itagi AV, Karns D, Peng W, Peng Y, Yang X, Zhu X, Gokemeijer NJ, Hsia YT, Ju G, Rottmayer RE, Seigler MA, Gage EC (2009) Heat-assisted magnetic recording by a near-field transducer with efficient optical energy transfer. *Nat. Photonics* 3: 220–224.

7. Kim S, Jin JH, Kim YJ, Park IY, Kim Y, Kim SW (2008) High-harmonic generation by resonant plasmon field enhancement. *Nature* 453: 757–760.
8. Nagatani N, Tanaka R, Yuhi T, Endo T, Kerman K, Takamura Y, Tamiya E (2006) Gold nanoparticle-based novel enhancement method for the development of highly sensitive immunochromatographic test strips. *Sci. Technol. Adv. Mater.* 7: 270–275.
9. Hirsch LR, Stafford RJ, Bankson JA, Sershen SR, Rivera B, Price RE, Hazle JD, Halas NJ, West JL (2003) Nanoshell-mediated near-infrared thermal therapy of tumors under magnetic resonance guidance. *Proc. Natl Acad. Sci. USA* 100: 13549–13554.
10. Park I-Y, Kim S, Choi J, Lee D-H, Kim Y-J, Kling MF, Stockman MI, Kim S-W (2011) Plasmonic generation of ultrashort extreme-ultraviolet light pulses. *Nat. Photonics* 5: 677–681.
11. Stockman MI (2011) Nanoplasmonics: the physics behind the applications. *Phys. Today* 64: 39–44.
12. Stockman MI (2011) Nanoplasmonics: past, present, and glimpse into future. *Opt. Express* 19: 22029–22106.
13. Kahng D (1963) Electric field controlled semiconductor device. US Patent 3,102,230.
14. Tsividis Y (1999) *Operation and Modeling of the MOS Transistor*. New York: McGraw-Hill.
15. Bergman DJ, Stockman MI (2003) Surface plasmon amplification by stimulated emission of radiation: quantum generation of coherent surface plasmons in nanosystems. *Phys. Rev. Lett.* 90: 027402.
16. Stockman MI, Bergman DJ (2009) Surface plasmon amplification by stimulated emission of radiation (spaser). US Patent 7,569,188.
17. Stockman MI (2008) Spasers explained. *Nat. Photonics* 2: 327–329.
18. Stockman MI (2010) The spaser as a nanoscale quantum generator and ultrafast amplifier. *J. Opt.* 12: 024004.
19. Stockman MI (2011) Spaser action, loss compensation, and stability in plasmonic systems with gain. *Phys. Rev. Lett.* 106: 156802.
20. Stockman MI (2011) Loss compensation by gain and spasing. *Phil. Trans. R. Soc. A* 369: 3510–3524.
21. Andrianov ES, Pukhov AA, Dorofeenko AV, Vinogradov AP, Lisyansky AA (2011) Dipole response of spaser on an external optical wave. *Opt. Lett.* 36: 4302–4304.
22. Campbell SD, Ziolkowski RW (2011) Impact of strong localization of the incident power density on the nano-amplifier characteristics of active coated nano-particles. *Opt. Commun.* doi: 10.1016/j.optcom.2011.11.006.
23. Lisyansky AA, Nechepurenko IA, Dorofeenko AV, Vinogradov AP, Pukhov AA (2011) Channel spaser: coherent excitation of one-dimensional plasmons from quantum dots located along a linear channel. *Phys. Rev. B* 84: 153409.
24. Liu SY, Li JF, Zhou F, Gan L, Li ZY (2011) Efficient surface plasmon amplification from gain-assisted gold nanorods. *Opt. Lett.* 36: 1296–1298.
25. Fedyanin DY (2012) Toward an electrically pumped spaser. *Opt. Lett.* 37: 404–406.

26. Andrianov ES, Pukhov AA, Dorofeenko AV, Vinogradov AP, Lisyansky AA (2012) Spaser chains. ArXiv: 1202.2925 [cond-mat.mes-hall].
27. Noginov MA, Zhu G, Belgrave AM, Bakker R, Shalaev VM, Narimanov EE, Stout S, Herz E, Suteewong T, Wiesner U (2009) Demonstration of a spaser-based nanolaser. *Nature* 460: 1110–1112.
28. Hill MT, Marell M, Leong ESP, Smalbrugge B, Zhu Y, Sun M, van Veldhoven PJ, Geluk EJ, Karouta F, Oei Y-S, Nötzel R, Ning C-Z, Smit MK (2009) Lasing in metal–insulator–metal sub-wavelength plasmonic waveguides. *Opt. Express* 17: 11107–11112.
29. Oulton RF, Sorger VJ, Zentgraf T, Ma R-M, Gladden C, Dai L, Bartal G, Zhang X, (2009) Plasmon lasers at deep subwavelength scale. *Nature* 461: 629–632.
30. Ma R-M, Oulton RF, Sorger VJ, Bartal G, Zhang X (2010) Room-temperature sub-diffraction-limited plasmon laser by total internal reflection. *Nat. Mater.* 10: 110–113.
31. Flynn RA, Kim CS, Vurgaftman I, Kim M, Meyer JR, Mäkinen AJ, Bussmann K, Cheng L, Choa FS, Long JP (2011) A room-temperature semiconductor spaser operating near 1.5 micron. *Opt. Express* 19: 8954–8961.
32. Wu CY, Kuo CT, Wang CY, He CL, Lin MH, Ahn H, Gwo S (2011) Plasmonic green nanolaser based on a metal-oxide-semiconductor structure. *Nano Lett.* 11: 4256–4260.
33. Marell MJH, Smalbrugge B, Geluk EJ, van Veldhoven PJ, Barcones B, Koopmans B, Nötzel R, Smit MK, Hill MT (2011) Plasmonic distributed feedback lasers at telecommunications wavelengths. *Opt. Express* 19: 15109–15118.
34. Sorger VJ, Zhang X (2011) Spotlight on plasmon lasers. *Science* 333: 709–710.
35. Ma RM, Oulton RF, Sorger VJ, Zhang X (2012) Plasmon lasers: coherent light source at molecular scales. *Laser Photonics Rev.* doi: 10.1002/lpor.201100040.
36. Berini P, Leon ID (2012) Surface plasmon-polariton amplifiers and lasers. *Nat. Photonics* 6: 16–24.
37. Leon ID, Berini P (2011) Measuring gain and noise in active long-range surface plasmon-polariton waveguides. *Rev. Sci. Instrum.* 82: 033107–10.
38. Ding K, Liu ZC, Yin LJ, Hill MT, Marell MJH, van Veldhoven PJ, Noetzel R, Ning CZ (2012) Room-temperature continuous wave lasing in deep-subwavelength metallic cavities under electrical injection. *Phys. Rev. B* 85: 041301.
39. Kwon S-H, Kang J-H, Kim S-K, Park H-G (2011) Surface plasmonic nanodisk/nanopan lasers. *IEEE J. Quantum Elect.* 47: 1346–1353.
40. Hill MT, Oei Y-S, Smalbrugge B, Zhu Y, de Vries T, van Veldhoven PJ, van Otten FWM, Eijkemans TJ, Turkiewicz JP, de Waardt H, Geluk EJ, Kwon S-H, Lee Y-H, Noetzel R, Smit MK (2007) Lasing in metallic-coated nanocavities. *Nat. Photonics* 1: 589–594.
41. Stockman MI, Faleev SV, Bergman DJ (2001) Localization versus delocalization of surface plasmons in nanosystems: can one state have both characteristics? *Phys. Rev. Lett.* 87: 167401.
42. Larkin IA, Stockman MI (2005) Imperfect perfect lens. *Nano Lett.* 5: 339–343.
43. Gordon JA, Ziolkowski RW (2007) The design and simulated performance of a coated nano-particle laser. *Opt. Express* 15: 2622–2653.

44. Bergman DJ, Stroud D (1992) Properties of macroscopically inhomogeneous media. In: Ehrenreich H, Turnbull D, editors. *Solid State Physics.* Vol. 46. Boston: Academic Press. pp 148–270.

45. Bergman DJ, Stroud D (1980) Theory of resonances in the electromagnetic scattering by macroscopic bodies. *Phys. Rev. B* 22: 3527–3539.

46. Plum E, Fedotov VA, Kuo P, Tsai DP, Zheludev NI (2009) Towards the lasing spaser: controlling metamaterial optical response with semiconductor quantum dots. *Opt. Express* 17: 8548–8551.

47. Seidel J, Grafstroem S, Eng L (2005) Stimulated emission of surface plasmons at the interface between a silver film and an optically pumped dye solution. *Phys. Rev. Lett.* 94: 177401.

48. Noginov MA, Zhu G, Mayy M, Ritzo BA, Noginova N, Podolskiy VA (2008) Stimulated emission of surface plasmon polaritons. *Phys. Rev. Lett.* 101: 226806.

49. Li K, Li X, Stockman MI, Bergman DJ (2005) Surface plasmon amplification by stimulated emission in nanolenses. *Phys. Rev. B* 71: 115409.

50. Dong ZG, Liu H, Li T, Zhu ZH, Wang SM, Cao JX, Zhu SN, Zhang X (2008) Resonance amplification of left-handed transmission at optical frequencies by stimulated emission of radiation in active metamaterials. *Opt. Express* 16: 20974–20980.

51. Wegener M, Garcia-Pomar JL, Soukoulis CM, Meinzer N, Ruther M, Linden S (2008) Toy model for plasmonic metamaterial resonances coupled to two-level system gain. *Opt. Express* 16: 19785–19798.

52. Fang A, Koschny T, Wegener M, Soukoulis CM (2009) Self-consistent calculation of metamaterials with gain. *Phys. Rev. B (Rapid Commun.)* 79: 241104(R).

53. Wuestner S, Pusch A, Tsakmakidis KL, Hamm JM, Hess O (2010) Overcoming losses with gain in a negative refractive index metamaterial. *Phys. Rev. Lett.* 105: 127401.

54. Chang SW, Ni CYA, Chuang SL (2008) Theory for bowtie plasmonic nanolasers. *Opt. Express* 16: 10580–10595.

55. Zheludev NI, Prosvirnin SL, Papasimakis N, Fedotov VA (2008) Lasing spaser. *Nat. Photonics* 2: 351–354.

56. Protsenko IE, Uskov AV, Zaimidoroga OA, Samoilov VN, O'Reilly EP (2005) Dipole nanolaser. *Phys. Rev. A* 71: 063812.

57. Ambati M, Nam SH, Ulin-Avila E, Genov DA, Bartal G, Zhang X (2008) Observation of stimulated emission of surface plasmon polaritons. *Nano Lett.* 8: 3998–4001.

58. Zhou ZK, Su XR, Peng XN, Zhou L (2008) Sublinear and superlinear photoluminescence from Nd doped anodic aluminum oxide templates loaded with Ag nanowires. *Opt. Express* 16: 18028–18033.

59. Noginov MA, Podolskiy VA, Zhu G, Mayy M, Bahoura M, Adegoke JA, Ritzo BA, Reynolds K (2008) Compensation of loss in propagating surface plasmon polariton by gain in adjacent dielectric medium. *Opt. Express* 16: 1385–1392.

60. Bolger PM, Dickson W, Krasavin AV, Liebscher L, Hickey SG, Skryabin DV, Zayats AV (2010) Amplified spontaneous emission of surface plasmon polaritons and limitations on the increase of their propagation length. *Opt. Lett.* 35: 1197–1199.

61. Chen Y-H, Li J, Ren M-L, Li Z-Y (2012) Amplified spontaneous emission of surface plasmon polaritons with unusual angle-dependent response. *Small*. doi: 10.1002/smll.201101806.
62. Noginov MA, Zhu G, Bahoura M, Adegoke J, Small C, Ritzo BA, Drachev VP, Shalaev VM (2007) The effect of gain and absorption on surface plasmons in metal nanoparticles. *Appl. Phys. B* 86: 455–460.
63. Noginov MA (2008) Compensation of surface plasmon loss by gain in dielectric medium. *J. Nanophotonics* 2: 021855.
64. Leon ID, Berini P (2010) Amplification of long-range surface plasmons by a dipolar gain medium. *Nat. Photonics* 4: 382–387.
65. Bergman DJ, Stroud D (1992) Properties of macroscopically inhomogeneous media. In: Ehrenreich H, Turnbull D, editors. *Solid State Physics*. Vol. 46. Boston: Academic Press. pp 148–270.
66. Stockman MI, Bergman DJ, Kobayashi T (2004) Coherent control of nanoscale localization of ultrafast optical excitation in nanosystems. *Phys. Rev. B* 69: 054202.
67. Landau LD, Lifshitz EM (1984) *Electrodynamics of Continuous Media.* Oxford: Pergamon.
68. Schawlow AL, Townes CH (1958) Infrared and optical masers. *Phys. Rev.* 112: 1940.
69. Johnson PB, Christy RW (1972) Optical constants of noble metals. *Phys. Rev. B* 6: 4370–4379.
70. De Angelis F, Das G, Candeloro P, Patrini M, Galli M, Bek A, Lazzarino M, Maksymov I, Liberale C, Andreani LC, Di Fabrizio E (2009) Nanoscale chemical mapping using three-dimensional adiabatic compression of surface plasmon polaritons. *Nat. Nanotechnol.* 5: 67–72.
71. Neacsu CC, Berweger S, Olmon RL, Saraf LV, Ropers C, Raschke MB (2010) Near-field localization in plasmonic superfocusing: a nanoemitter on a tip. *Nano Lett.* 10: 592–596.
72. Atwater HA, Polman A (2010) Plasmonics for improved photovoltaic devices. *Nat. Mater.* 9: 205–213.
73. Kneipp K, Moskovits M, Kneipp H, editors (2006) *Surface Enhanced Raman Scattering: Physics and Applications*. Heidelberg: Springer-Verlag.
74. Kneipp J, Kneipp H, Wittig B, Kneipp K (2010) Novel optical nanosensors for probing and imaging live cells. *Nanomed. Nanotechnol. Biol. Med.* 6: 214–226.
75. Stockman MI (2006) Electromagnetic theory of SERS. In: Moskovits M, Kneipp K, Kneipp H, editors. *Surface Enhanced Raman Scattering*. Vol. 103. Heidelberg: Springer-Verlag. pp 47–66.
76. Dunmore FJ, Liu DZ, Drew HD, Dassarma S, Li Q, Fenner DB (1995) Observation of below-gap plasmon excitations in superconducting YBa2Cu3O7 films. *Phys. Rev. B* 52: R731–R734.
77. Schumacher D, Rea C, Heitmann D, Scharnberg K (1998) Surface plasmons and Sommerfeld-Zenneck waves on corrugated surfaces: application to high-T_c superconductors. *Surf. Sci.* 408: 203–211.

78. Fedotov VA, Tsiatmas A, Shi JH, Buckingham R, deGroot P, Chen Y, Wang S, Zheludev NI (2010) Temperature control of Fano resonances and transmission in superconducting metamaterials. *Opt. Express* 18: 9015–9019.

79. Tsiatmas A, Buckingham AR, Fedotov VA, Wang S, Chen Y, deGroot PAJ, Zheludev NI (2010) Superconducting plasmonics and extraordinary transmission. *Appl. Phys. Lett.* 97: 111106.

80. Anlage SM (2011) The physics and applications of superconducting metamaterials. *J. Opt.* 13: 024001.

81. Boltasseva A, Atwater HA (2011) Low-loss plasmonic metamaterials. *Science* 331: 290–291.

82. Shalaev VM (2007) Optical negative-index metamaterials. *Nat. Photonics* 1: 41–48.

83. Zheludev NI (2011) A roadmap for metamaterials. *Opt. Photonics News* 22: 30–35.

84. Bloch F (1929) Über die Quantenmechanik der Elektronen in Kristallgittern. *Z. Phys. A* 52: 555–600.

85. Stockman MI, Kurlayev KB, George TF (1999) Linear and nonlinear optical susceptibilities of Maxwell Garnett composites: dipolar spectral theory. *Phys. Rev. B* 60: 17071–17083.

86. Li X, Stockman MI (2008) Highly efficient spatiotemporal coherent control in nanoplasmonics on a nanometer-femtosecond scale by time reversal. *Phys. Rev. B* 77: 195109.

87. Stockman MI, Pandey LN, George TF (1996) Inhomogeneous localization of polar eigenmodes in fractals. *Phys. Rev. B* 53: 2183–2186.

88. Stockman MI (2004) Nanofocusing of optical energy in tapered plasmonic waveguides. *Phys. Rev. Lett.* 93: 137404.

89. Xiao S, Drachev VP, Kildishev AV, Ni X, Chettiar UK, Yuan H-K, Shalaev VM (2010) Loss-free and active optical negative-index metamaterials. *Nature* 466: 735–738.

90. Gryczynski Z, Abugo OO, Lakowicz JR (1999) Polarization sensing of fluorophores in tissues for drug compliance monitoring. *Anal. Biochem.* 273: 204–211.

91. Merlin R (2009) Metamaterials and the Landau-Lifshitz permeability argument: large permittivity begets high-frequency magnetism. *Proc. Natl Acad. Sci. USA* 106: 1693–1698.

92. Meinzer N, Ruther M, Linden S, Soukoulis CM, Khitrova G, Hendrickson J, Olitzky JD, Gibbs HM, Wegener M (2010) Arrays of Ag split-ring resonators coupled to InGaAs single-quantum-well gain. *Opt. Express* 18: 24140–24151.

93. Kretschmann E, Raether H (1968) Radiative decay of nonradiative surface plasmons excited by light. *Z. Naturforsch. A* 23: 2135–2136.

94. Kitur JK, Podolskiy VA, Noginov MA (2011) Stimulated emission of surface plasmon polaritons in a microcylinder cavity. *Phys. Rev. Lett.* 106: 183903.

95. Hess O, Wuestner S, Pusch A, Tsakmakidis KL, Hamm JM (2011) Gain and plasmon dynamics in active negative-index metamaterials. *Phil. Trans. R. Soc. A* 369: 3525–3550.

96. Ghafouri-Shiraz H (2003) *Distributed Feedback Laser Diodes and Optical Tuneable Filters*. West Sussex, UK: John Wiley & Sons Ltd.

97. Stockman MI (2011) Reply to comment on "Spaser action, loss compensation, and stability in plasmonic systems with gain". *Phys. Rev. Lett.* 107: 259704.

98. Pendry JB, Maier SA (2011) Comment on "Spaser action, loss compensation, and stability in plasmonic systems with gain". *Phys. Rev. Lett.* 107: 259703.

99. Anderson PW (1958) Absence of diffusion in certain random lattices. *Phys. Rev.* 109: 1492–1505.

100. Tsai DP, Kovacs J, Wang Z, Moskovits M, Shalaev VM, Suh JS, Botet R (1994) Photon scanning tunneling microscopy images of optical excitations of fractal metal colloid clusters. *Phys. Rev. Lett.* 72: 4149–4152.

101. Stockman MI, Pandey LN, Muratov LS, George TF (1995) Photon scanning-tunneling-microscopy images of optical-excitations of fractal metal colloid clusters—comment. *Phys. Rev. Lett*. 75: 2450–2450.